Arctic Science

OPEN ACCESS | Article

Cumulative impacts of a gravel road and climate change in an ice-wedge-polygon landscape, Prudhoe Bay, Alaska

Donald A. Walker[a,b], **Martha K. Raynolds**[b], **Mikhail Z. Kanevskiy**[c], **Yuri S. Shur**[c,d], **Vladimir E. Romanovsky**[e,f], **Benjamin M. Jones**[c], **Marcel Buchhorn**[g], **M. Torre Jorgenson**[h], **Jozef Šibík**[i], **Amy L. Breen**[a,j], **Anja Kade**[a], **Emily Watson-Cook**[a], **Georgy Matyshak**[k], **Helena Bergstedt**[c,l], **Anna K. Liljedahl**[m], **Ronald P. Daanen**[n], **Billy Connor**[c,o], **Dmitry Nicolsky**[f], **and Jana L. Peirce**[b]

[a]University of Alaska Fairbanks, Department of Biology and Wildlife, Fairbanks, Alaska, USA, 99775; [b]University of Alaska Fairbanks, Institute of Northern Engineering, Fairbanks, Alaska, USA, 99775; [c]Department of Geology and Geophysics, University of Alaska Fairbanks, Geophysical Institute, Fairbanks, Alaska, USA, 99775; [d]University of Alaska Fairbanks, Department of Civil Engineering, Fairbanks, Alaska, USA, 99775; [e]University of Alaska Fairbanks, Geophysical Institute, Fairbanks, Alaska, USA, 99775; [f]University of Alaska, Department of Geology and Geophysics, Fairbanks, Alaska, USA, 99775; [g]Flemish Institute for Technological Research (VITO), Mol, Belgium, BE-2400; [h]Alaska Ecoscience, Fairbanks, Alaska, USA, 99709; [i]Institute of Botany, Slovak Academy of Sciences, Plant Science and Biodiversity Center of Bratislava, Slovak Republic, SK845 23; [j]University of Alaska Fairbanks, International Arctic Research Center, Fairbanks, Alaska, USA, 99775; [k]Lomonosov Moscow State University, Soil Science Department, Moscow, Russia, 119991; [l]B.geos GmbH, Korneburg, Austria, 2100; [m]Woodwell Climate Research Center, Falmouth, Massachusetts, USA, 02540; [n]Alaska Division of Geological & Geophysical Surveys, Fairbanks, Alaska, USA, 99775; [o]University of Alaska Fairbanks, Arctic Infrastructure Development Center, Fairbanks, Alaska, USA, 99775

Corresponding author: **Donald A. Walker** (email: dawalker@alaska.edu)

Abstract

Environmental impact assessments for new Arctic infrastructure do not adequately consider the likely long-term cumulative effects of climate change and infrastructure to landforms and vegetation in areas with ice-rich permafrost, due in part to lack of long-term environmental studies that monitor changes after the infrastructure is built. This case study examines long-term (1949–2020) climate- and road-related changes in a network of ice-wedge polygons, Prudhoe Bay Oilfield, Alaska. We studied four trajectories of change along a heavily traveled road and a relatively remote site. During 20 years prior to the oilfield development, the climate and landscapes changed very little. During 50 years after development, climate-related changes included increased numbers of thermokarst ponds, changes to ice-wedge-polygon morphology, snow distribution, thaw depths, dominant vegetation types, and shrub abundance. Road dust strongly affected plant-community structure and composition, particularly small forbs, mosses, and lichens. Flooding increased permafrost degradation, polygon center-trough elevation contrasts, and vegetation productivity. It was not possible to isolate infrastructure impacts from climate impacts, but the combined datasets provide unique insights into the rate and extent of ecological disturbances associated with infrastructure-affected landscapes under decades of climate warming. We conclude with recommendations for future cumulative impact assessments in areas with ice-rich permafrost.

Key words: flooding, landforms, permafrost, road dust, thermokarst, vegetation

Résumé

Les évaluations des impacts environnementaux des nouvelles infrastructures dans l'Arctique ne tiennent pas suffisamment compte des effets cumulatifs probables à long terme des changements climatiques et des infrastructures sur les formes de relief et la végétation dans les régions où le pergélisol est riche en glace. Cela est dû en partie au manque d'études environnementales à long terme qui suivent les changements après la construction des infrastructures. Cette étude de cas examine les changements à long terme (1949–2020) liés au climat et aux routes dans un réseau de polygones de toundra, le Prudhoe Bay Oilfield, en Alaska. Les auteurs ont étudié quatre trajectoires de changements le long d'une route très fréquentée et sur un site relativement éloigné. Pendant les 20 années précédant l'exploitation du champ pétrolifère, le climat et les paysages ont très peu changé. Pendant les 50 ans qui ont suivi l'exploitation, les changements liés au climat comprenaient une augmentation

du nombre d'étangs thermokarstiques, des changements dans la morphologie des polygones de toundra, la distribution de la neige, les profondeurs de dégel, les types dominants de végétation et l'abondance des arbustes. La poussière des routes a fortement affecté la structure et la composition des communautés végétales, en particulier les petites plantes herbacées non graminoïdes, les mousses et les lichens. Les inondations ont augmenté la dégradation du pergélisol, les contrastes d'élévation entre le centre et le creux des polygones, et la productivité de la végétation. Il n'a pas été possible d'isoler les impacts des infrastructures des impacts climatiques, mais les ensembles de données combinés fournissent des informations uniques sur le taux et l'étendue des perturbations écologiques associées aux paysages affectés par les infrastructures pendant des décennies de réchauffement climatique. Les auteurs concluent avec des recommandations pour les futures évaluations des impacts cumulatifs dans les zones à pergélisol riche en glace. [Traduit par la Rédaction]

Mots-clés : inondation, formes de terrain, pergélisol, poussière de route, thermokarst, végétation

Introduction

Nearly all roads and most permanent infrastructure in northern Alaska are built on thick gravel pads (Ferrians et al. 1969). The pads are needed to protect structures from thermokarst and thermal erosion of the permafrost beneath them, but they also alter the hydrology and snow patterns, add large volumes of dust to adjacent ecosystems, and promote a variety of other roadside impacts that cause complex cumulative impacts to the underlying permafrost and adjacent ecosystems. These impacts have been studied separately to some extent in previous studies of road-related impacts in northern Alaska (e.g., Benson et al. 1975; Everett and Parkinson 1977; Brown and Berg 1980; Everett 1980*a*;Auerbach et al. 1997; Kidd et al. 2006; Myers-Smith et al. 2006; Gill et al. 2014; Walker and Peirce 2015; Raynolds et al. 2014*a*, 2020; Ackerman and Finley 2019; Connor et al. 2020; Schneider von Deimling et al. 2021; Kanevskiy et al. 2022). Here we examine the combined cumulative effects of road- and climate-related changes of a gravel road in an area of ice-rich permafrost.

This study was prompted by numerous observations that have documented recent rapid ice-wedge degradation and thermokarst in northern Alaska and much of the circumpolar Arctic due to climate warming (Jorgenson et al. 2006, 2015*a*, 2018; Godin et al. 2014, 2016; Perreault et al. 2016; Raynolds et al. 2014; Liljedahl et al. 2016; Kanevskiy et al. 2017, 2022; Fraser et al. 2018; Frost et al. 2018; Farquharson et al. 2019). Thermokarst refers to the process by which thawing of ice-rich permafrost or melting of massive ground ice creates subsidence of the ground surface and irregular topography consisting of characteristic landforms, such as thermokarst pits, ponds, lakes, mounds, and high-centered polygons (Fig. 1) (Jones et al. 2013; Kanevskiy et al. 2022). The economic impact of thermokarst-related degradation related to Arctic roads has long been recognized (e.g., Nelson et al. 2001; Melvin et al. 2017; Romanovsky et al. 2017). Efforts are being made to develop engineering solutions to reduce the impacts to infrastructure (e.g., Schneider von Deimling et al. 2021), but the long-term cumulative impacts of road-related and climate-related impacts to permafrost, landforms, and vegetation in adjacent Arctic ecosystems remain poorly studied and are not adequately considered during the planning process for new roads.

Understanding the cumulative impacts of Arctic roads and climate change is especially important for cumulative impact assessments for new infrastructure in areas that have high conservation value and/or high subsistence value to local people. For example, a recent environmental impact assessment that examined potential effects of a proposed petroleum-exploration leasing program in the Arctic National Wildlife Refuge in northern Alaska (BLM 2019) was criticized for lack of attention to potential cumulative impacts that would likely follow leasing, including impacts from seismic surveys, exploration drilling, oilfield infrastructure, and climate change (Raynolds et al. 2020). The Department of Interior suspended all activities related to implementation of leasing activities in the ANWR pending completion of a supplemental analysis (DOI 2021).

The U.S. Council on Environmental Quality (CEQ) defines cumulative impacts (CIs) as:

> "…the impact on the environment which results from the incremental impact of the action when added to other past, present and reasonably foreseeable future actions, regardless of what agency (federal or non-federal) or person undertakes such other action. Cumulative impacts can result from individually minor but collectively significant actions taking place over a period of time." (CEQ 1997).

Similar definitions are used in Canada (Beanlands and Duinker 1983) and Europe (EC 1999). Cumulative impact assessments (CIAs) are often mandated for large infrastructure projects in USA as part of the environmental impact assessment process defined by the National Environmental Policy Act and amendments (42 U.S. Code §431 et seq. 1969). Several Arctic countries have similar laws regarding CIAs (Connelly 2011).

CIs are difficult to predict because of the complexity of ecological interactions, the scarcity of environmental baseline data, and the difficulty in defining the spatial and temporal boundaries for meaningful assessments (Clark 1994). Objective rules for conducting CIAs are also generally lacking, including how to include substantive public engagement, monitoring, adaptive management, and conflicting land-management objectives from national, state, and local agencies (Jones 2016). CIAs are generally not integrated into comprehensive regional planning processes, so it is difficult to follow through on recommendations generated by a CIA (NRC 2003). Nonetheless, CIAs are often mandated for large projects despite these difficulties because of the potential large long-term consequences that would likely occur in the absence of a thorough consideration of interactions between multiple sources of likely impacts over long periods of time.

Fig. 1. Roadside area through a network of ice-wedge polygons, Prudhoe Bay Oilfield, Alaska. Roadside flooding, road dust, and other impacts have caused subsidence of the ice-wedges and erosion of the polygon centers. Here, low-centered polygons have been converted to high-centered polygons, altering ecosystems in a wide swath of tundra adjacent to the road.

The objective of this paper is to document 70 years (1949–2019) of cumulative effects of climate- and road-related impacts of a heavily traveled road in the Prudhoe Bay Oilfield (PBO) with an aim toward improving CIAs for future roads. We focus on the often-ignored indirect impacts that follow the direct impact or footprint of new roads. Indirect impacts related to roads include interactions between climate change, road dust, roadside flooding, and other roadside impacts.

Our evaluation of cumulative impacts included: (1) examination of change along four impact trajectories with increasing levels of impact, (2) mapping studies, (3) transect-based studies, and (4) plot-based studies. We present the results from each method, discuss changes to landforms and vegetation in each trajectory of change, and conclude with recommendations for future CIAs for roads and related infrastructure in ice-rich permafrost landscapes.

This study addresses the core system-level themes (thresholds, connectivity, and emergent properties) of T-MOSAiC (Terrestrial Multidisciplinary distributed Observatories for the Study of Arctic Connections) (Vincent et al. 2019) and has strong relevance to the implications of infrastructure changes for Arctic social systems (Vincent et al. 2017; Povoroznyuk et al. 2021).

Methods

Regional description

The PBO was discovered in 1967 and was the first of a series of North Slope oilfields that are concentrated in approximately 1300 km^2 of the Arctic Coastal Plain, Alaska (Fig. 2*a*) (Truett and Johnson 2000; NRC 2003). Early development in the PBO occurred without baseline environmental studies and prior to the requirement for CIAs. The first comprehensive assessment of the environmental and social impacts of North Slope oilfields was conducted 36 years after PBO was discovered (NRC 2003). Forty-eight years of environmental studies in the PBO provided plot and map data for examining CIs at regional and landscape scales (e.g., Walker et al. 1986, 1987*b*; Maki 1992; Jorgenson and Joyce 1994; NRC 2003; Kidd et al. 2006; Streever et al. 2011; Raynolds et al. 2014*a*; Walker 1996).

Most of the PBO lies between the Sagavanirktok and Kuparuk rivers and is underlain by thick alluvial deposits associated with abandoned braided-river floodplains that are ancestral to present-day rivers (Rawlinson 1993; Jorgenson et al. 2018). The dominant landscape features include thaw lakes, drained thaw-lake basins, braided river floodplains, and ice-wedge polygons (Jorgenson 2011). Ice wedges of Holocene age dominate the upper 3–4 m of sediments. The topmost

Fig. 2. (*a*) The North Slope oilfields and major infrastructure, 2010. Red lines: gravel roads, airstrips, and construction pads. Green lines: major pipelines. Note the gray dashed boundary of the Prudhoe Bay Oilfield (PBO) and the Lake Colleen area (green box), the focus area for this study. The Dalton Highway and Trans-Alaska Pipeline System (TAPS) connect to Fairbanks and the marine terminal at Valdez, AK. Base map courtesy of BP Exploration-Alaska. (*b*) Lake Colleen and the Deadhorse service area. The infrastructure includes roads, two drill sites, and oilfield support facilities. Permafrost research has been conducted at the Jorgenson and Colleen sites. The Colleen site is located along a straight section of the Spine Road. The image is a false-color infrared image derived from satellite data Google Earth, 7/9/2010, ©Maxar Technologies 2020.

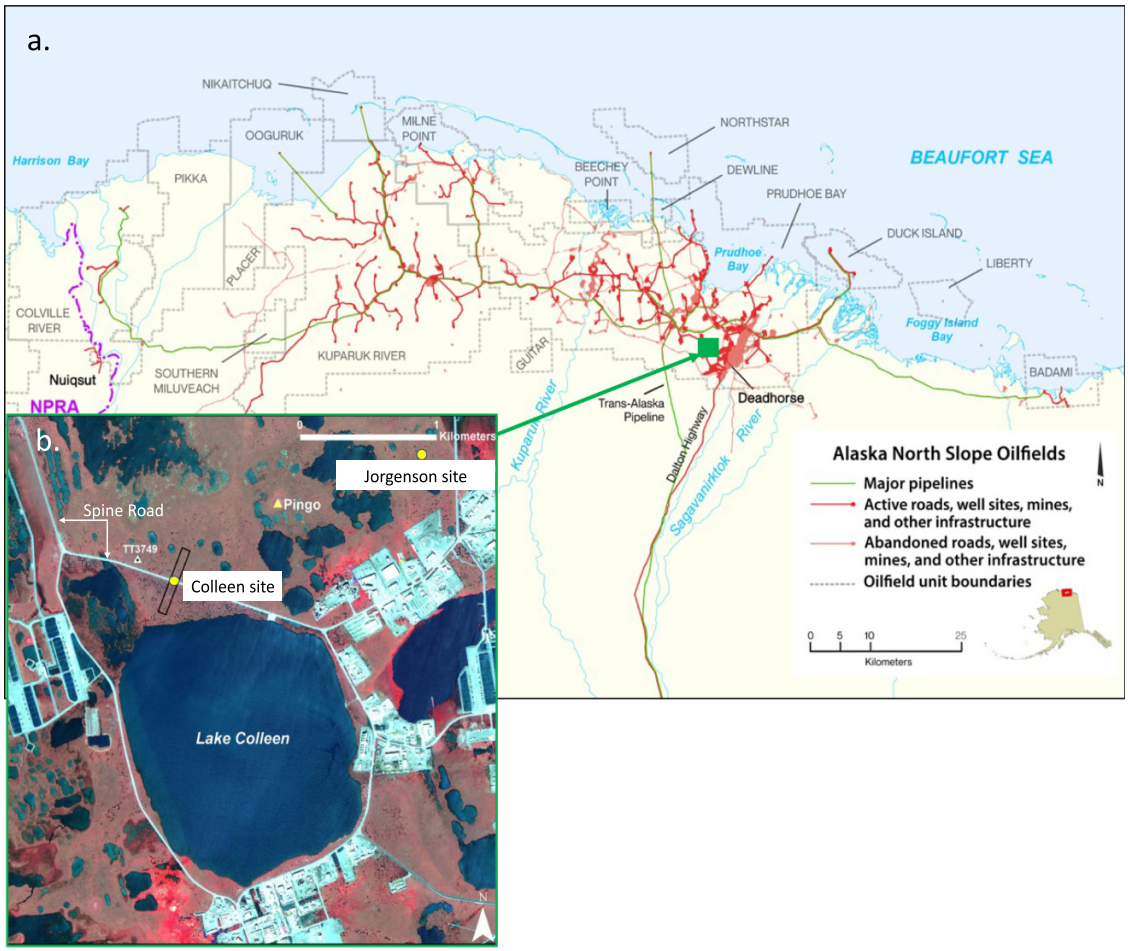

approximately 0.5-m layer of annually thawed peat and eolian silt is underlain by approximately 1.5–2 m of ice-rich and organic-rich silt that lies on top of the Quaternary-age alluvial gravels (Everett 1980*b*).

Study sites

The Colleen site (CS) (Figs. 2*b* and 3) was initiated in 2014 to analyze road-related impacts to terrain, vegetation, and permafrost (Walker et al. 2015, 2018). The Jorgenson site was created in 2011 to better understand the processes of ice-wedge degradation and stabilization (Jorgenson et al. 2015*a*). The CS and JS are on the same geomorphic surface that was mapped as a flat plain with a mosaic of primarily wet and moist nonacidic tundra plant communities and soils typical of low-centered polygons in the PBO (Everett et al. 1980). The common plant communities and habitats are described in Table S2.1.

The Colleen Site straddles the Spine Road (Fig. 3*a*) where it passes through an area of well-developed ice-wedge polygons on the north side of Lake Colleen (Fig. 2*b*). Transects T1 and T2 were surveyed to examine variation in the permafrost, vegetation, and environmental factors in polygon centers and troughs along 200-m swaths on both sides of the Spine Road. The T1 side of the road was most noticeably impacted by road dust and thermokarst (Fig. 3*b*). The T2 side was strongly affected by thermokarst, road dust, and flooding (Fig. 3*c*). Details of the sampling design and vegetation-analysis methods are in Supplemental file S2 and two data reports (Walker et al., 2015, 2018). A profile of the Colleen site is in Fig. S2.6 (Buchhorn et al. 2014). Details and discussion of the permafrost-related issues are described in (Kanevskiy et al. 2017, 2022).

The Jorgenson Site (JS) is located 1.8 km NE of the CS (Fig. 4) and is relatively isolated from road-related impacts. Changes to the ice-wedges, thermokarst ponds, and terrain topography at the JS between 1949 and 2012 have been described

Fig. 3. Colleen site (CS). (*a*) Digital false-color infrared aerial photograph (9 August 2010) of the 200-m transects (white lines) T1 (NE side of the road) and T2 (SW side). Paired vegetation plots (open white squares on the left side of the transects as one faces the transect from the road) are in polygon troughs (t) and polygon centers (c) at approximately 5, 10, 25, 50, 100, and 200 m from the road. Permafrost boreholes (open white circles on the right side of the transects) are in troughs and centers at similar distances from the road. (Base photo: Quantum Spatial, Anchorage, AK, permission courtesy of BP Alaska Prudhoe Bay Unit). (*b*) Ground view of Transect T1 in 2014. This is the relatively well-drained NE side of the road, and heavy road dust is apparent. Pin flags at 1-m intervals are for periodic monitoring of vegetation and environmental factors. (*c*) Transect T2 on the flooded SW side of the road, where the troughs between polygons are eroded and filled with water. The white 1.5-m stake is for locating the position of the transect during winter. Similar stakes are located at 0 m, 25 m, 50 m, 100 m, and 200 m from the road on both transects.

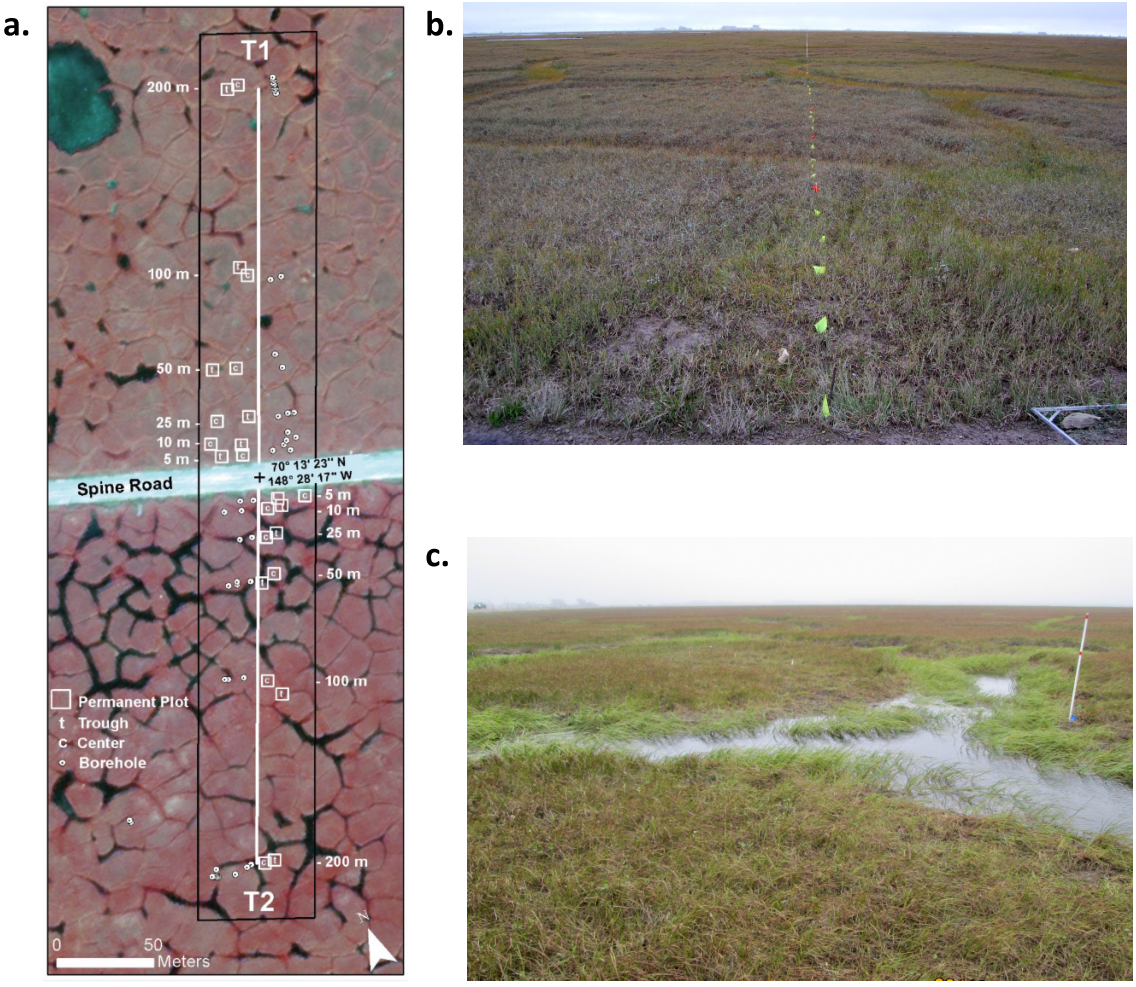

in two publications (Jorgenson et al. 2015*a*; Kanevskiy et al. 2017).

The JS and CS have similar well-developed ice-wedge polygons with large ice-wedges. The spacing of the ice-wedges along the JS and CS transects averages 13–15 m. Ice-wedge dimensions are highly variable with an average width of 3.0 ± 1.0 m at the top of the wedges and an average height of 3.3 ± 0.2 m (Jorgenson et al. 2015*a*). Abundant segregated ice, such as lenses and more complex forms, occurs in the sediments between ice-wedges (Kanevskiy et al. 2022). At the Jorgenson site (JS) (Fig. 2*b*), the estimated volume of wedge ice in the upper 3 m was 21%, determined from 83 boreholes (Kanevskiy et al. 2017). The estimated average total volumetric ice content (including wedge ice, segregated ice, and pore ice) in the upper 3 m of permafrost in bluffs along the Beaufort Sea coast was 77% (Kanevskiy et al. 2013).

Prior to 1968, the ice wedges beneath most troughs were obscured by soil and vegetation. Thermokarst ponds occurred at the intersection of only a few ice wedges (Figs. 3*a* and 4, 1949 and 1968 photos). By 2012, the tops of many ice wedges had thawed, and soils in the troughs had settled several centimeters allowing water to partially fill many troughs. Figure 3*c* is a ground-level view of polygon centers and water-filled troughs along CS transect T2 in 2014. Nearly, all the ponds shown on the 1949 images of the JS and CS are also present in the latest images. (See Figure 7 for 1949 and 2018 images of the Colleen site).

Fig. 4. Jorgenson site (JS) in 1968 and 2012. The white line is the 350-m JS transect. Studies of permafrost dynamics focused along the transect. Data reported here are from the 0 m–250 m section of the transect. Note the few thermokarst "pits" or ponds in the 1968 image. These occur mostly at the intersection of ice-wedges that lie beneath the troughs that separate adjacent ice-wedge polygons. The expansion of waterbodies In the 2012 image occurred where the soil surface in the ice-wedge-polygon troughs subsided due to partial melting of the ice-wedges, and the troughs became filled with water. Ice wedges lie below the waterbodies and nonflooded troughs. Details of the landscape and permafrost transitions are described by Jorgenson et al. (2015*a*) and Kanevskiy et al. (2017, 2021).

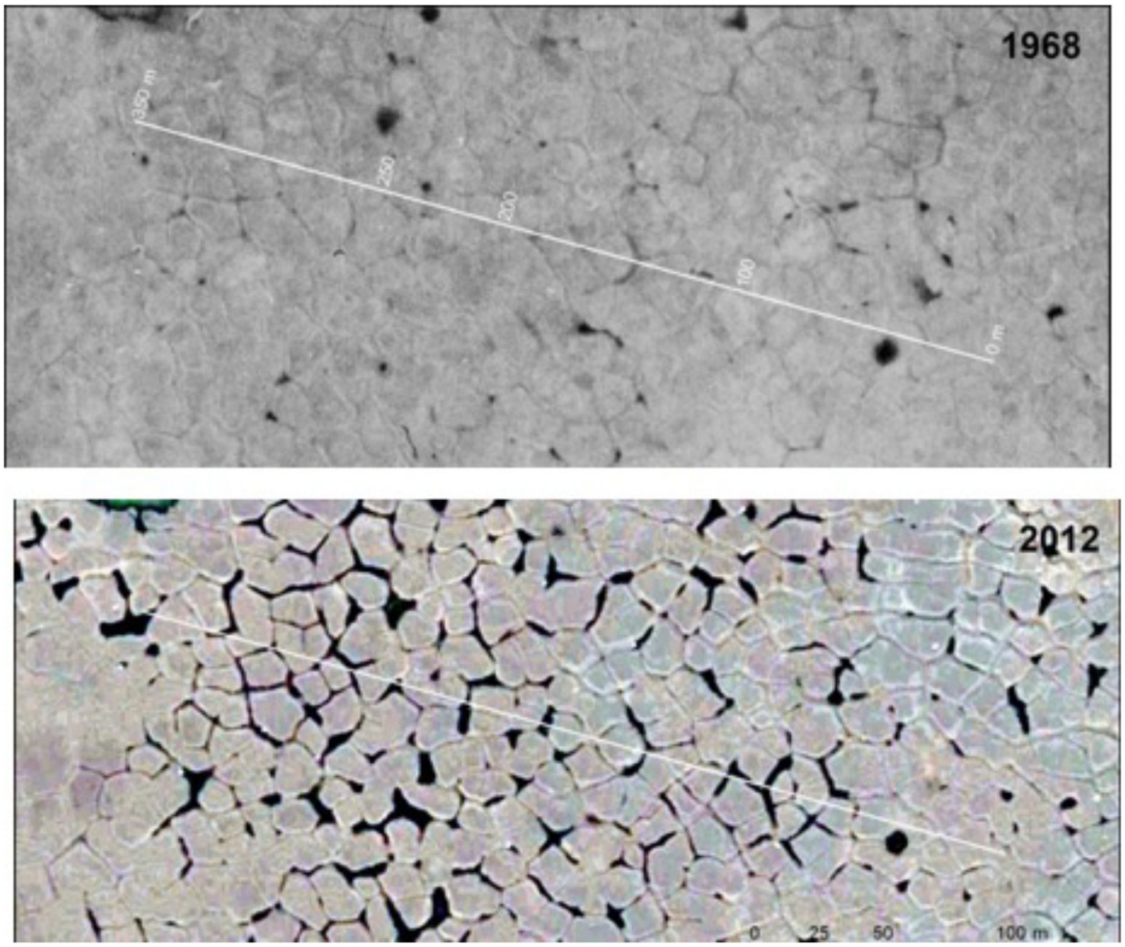

Baseline data

Aerial images

The oil industry and Quantum Spatial Inc (Anchorage) maintain an archive of aerial images of the PBO that includes images taken most years between 1968 and the present. Images of the JS from eight dates (1949, 1968, 1982,1988, 1997, 2004, 2009, and 2012) were analyzed during previous studies (Jorgenson et al. 2015*a*). For the Colleen site, we acquired digital copies of images from 1949 (U.S. Navy BAR) and 39 dates between 1968 and 2014 (BP Exploration Alaska, BPXA). We cropped them to an area centered on the CS transects and displayed them at a consistent scale (Fig. S1.1).

Geoecological studies

Ecological investigations were conducted in the Prudhoe Bay region during the 1970s as part of the US Tundra Biome–International Biological Program (Brown 1975; Webber and Walker 1975; Everett and Parkinson 1977; Everett 1980*b*, *c*, *d*; Everett et al. 1978; Walker and Webber 1980; Walker et al. 1980; Walker 1985; Walker and Everett 1991). The studies provide plot data and maps for the period prior to the recent rapid warming when geoecological conditions were still like those before oilfield development.

Climate

Mean annual air temperatures (MAAT), mean annual permafrost temperatures at 20-m depth (MAPT), and annual active-layer thicknesses (ALT) (Fig. 5*a*) were obtained from the Romanovsky Deadhorse site (https://permafrost.gi.alaska.edu/site/dh1) (Romanovsky and Osterkamp 1995; Romanovsky et al. 2017). The summer warmth index (SWI, Fig. 5*b*), the annual sum of the monthly mean temperatures > 0°C or "thawing degree months" (°C mo), was calculated using monthly mean-temperature data from two nearby stations that covered the

Fig. 5. Prudhoe Bay climate and thaw-depth trends: (*a*) Brown line: Active layer thickness (ALT, 1988–2019). Black line: mean annual permafrost temperature (MAPT, 1978–2019). Orange line: mean annual air temperature (MAAT, 1986–2019). Data are from Romanovsky's Deadhorse site (**https://permafrost.gi.alaska.edu/site/dh1**) (*b*) Red line: Summer warmth index (SWI = Annual sum of the monthly mean temperatures above freezing). The SWI graph combines two records from the Prudhoe (ARCO) Station (1969–1985; **Thoman 1995**) and the Deadhorse NWS Station (1986–2019, Western Regional Climate Center) (see Fig. 2 for locations). c. Precipitation (1983–2019. Light blue line: Annual precipitation; Dark blue line: Summer (JJA) precipitation (1983–2019). (*d*) Gray line: Annual snowfall (1982–1983 to 2019–2020). Data for *c* and *d* are from the Kuparuk Station (WRCC Station ID 505136). Red dashed vertical lines: Warm summers in 1989, 1998, and 2012.

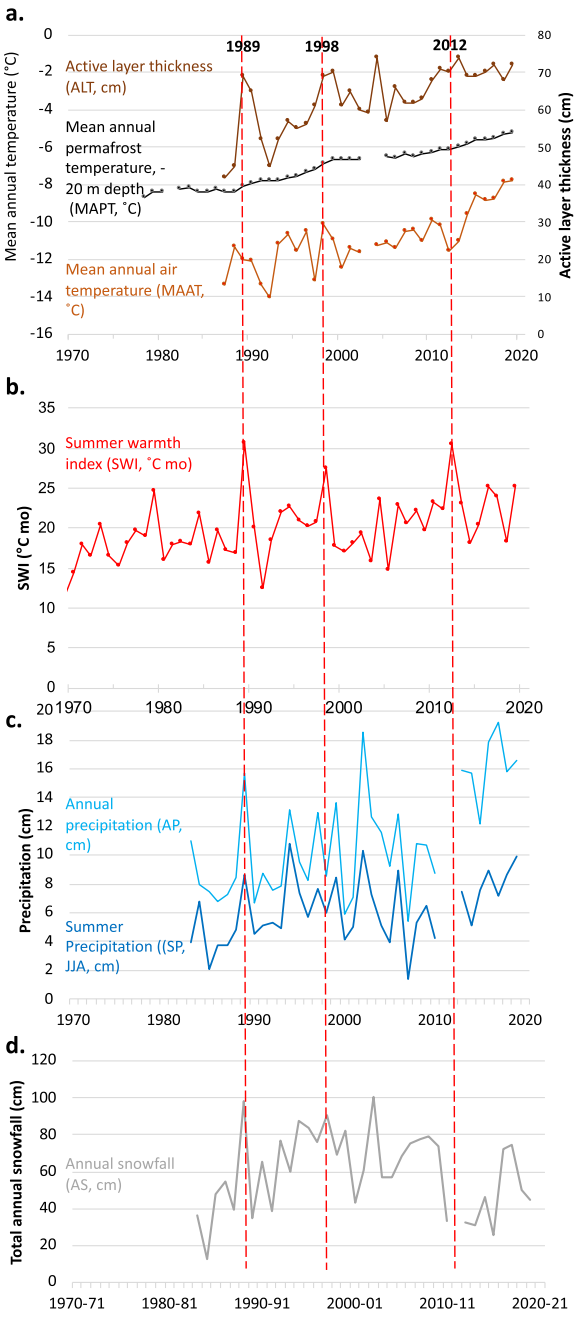

full period of oilfield development: Prudhoe Bay (ARCO) Station (1969–1985) (Western Regional Climate Center, http://scacis.rcc-acis.org/) and the Deadhorse Station (1986–2019) (Thoman 1995). Precipitation data (Fig. 5*c, d*) came from the Kuparuk Station, 47 km west of Deadhorse.

Impact evaluation methods

Cumulative impact trajectories

We studied four trajectories of increasing cumulative impacts (Fig. 6). Trajectory A examined conditions prior to road construction (1949–1968) using historical aerial photographs and literature sources from before and shortly after the Spine Road was constructed in 1969. Trajectory B assessed the impacts of climate change after discovery of the oilfield (1969–present) based mainly on data from the JS, which is relatively isolated from road-related effects. Trajectory C focused on the climate and dust impacts after road construction (1969–present) on the northeast, nonflooded side of the road (CS-T2). Trajectory D examined the impacts of climate change, road dust, and flooding on the southwest, flooded, side of the road (CS-T2). An overview of the mapping, plot-based studies, transect-based studies, and analytical methods are shown in Fig. S2.1.

Mapping studies

Waterbodies

The impacts of flooding were assessed from maps of waterbody distribution at the JS and CS. At the JS, a time series of eight aerial photographs were analyzed using air-photo interpretation for changes in waterbody distribution (Jorgenson et al. 2015*a*). For the CS, we selected ten images from the collection of images in Fig. S1.1 spaced at 3–7-year intervals between 1968 and 2013 plus a 2018 Worldview-2 satellite image. The spatial resolution of the images ranged from 0.05 to 0.38 m and were resampled to 0.40 m before processing. The ponds were separated based on their distinctive dark tones and shapes on the aerial photos. The software eCognition® (Trimble Geospatial), an object-based analysis tool, aided in the separation and calculation of the area of waterbodies.

Vegetation change

Vegetation at the CS was mapped using image interpretation of digital versions of aerial photographs taken in 1972 and 2013 and the Iso Cluster unsupervised classification approach of the ENVI® classification software (L3Harris Geospatial). We grouped the image pixels according to the vegetation units of the cluster analysis (described below) plus a barren category to represent the road and barren areas next to the road. The vegetation units were based on prior vegetation classes developed for previous vegetation mapping (Walker and Webber 1980) (Table S2.1).

Transect-based studies

At the Jorgenson Site, a 350-m transect was surveyed in 2013, and subsequent studies were concentrated from 0 to 250 m (Fig. 4). The methods and results of these studies are

Fig. 6. Four trajectories of change due to cumulative impacts of climate change and road-related impacts at the Jorgenson and Colleen sites. (*a*) Pre-road before rapid climate change (1949–1968); interpreted mainly from aerial photographs, geobotanical maps, and ground observations by the IBP Tundra Biome in the 1970s; (*b*) Climate change and no road (1969–present), interpreted mainly from information at the JS; (*c*) Climate change and road dust (1969–present), interpreted mainly from CS T1; and d) Climate change, road dust, and flooding interpreted mainly from CS T2. The trajectories represent a gradient of increasing cumulative impacts.

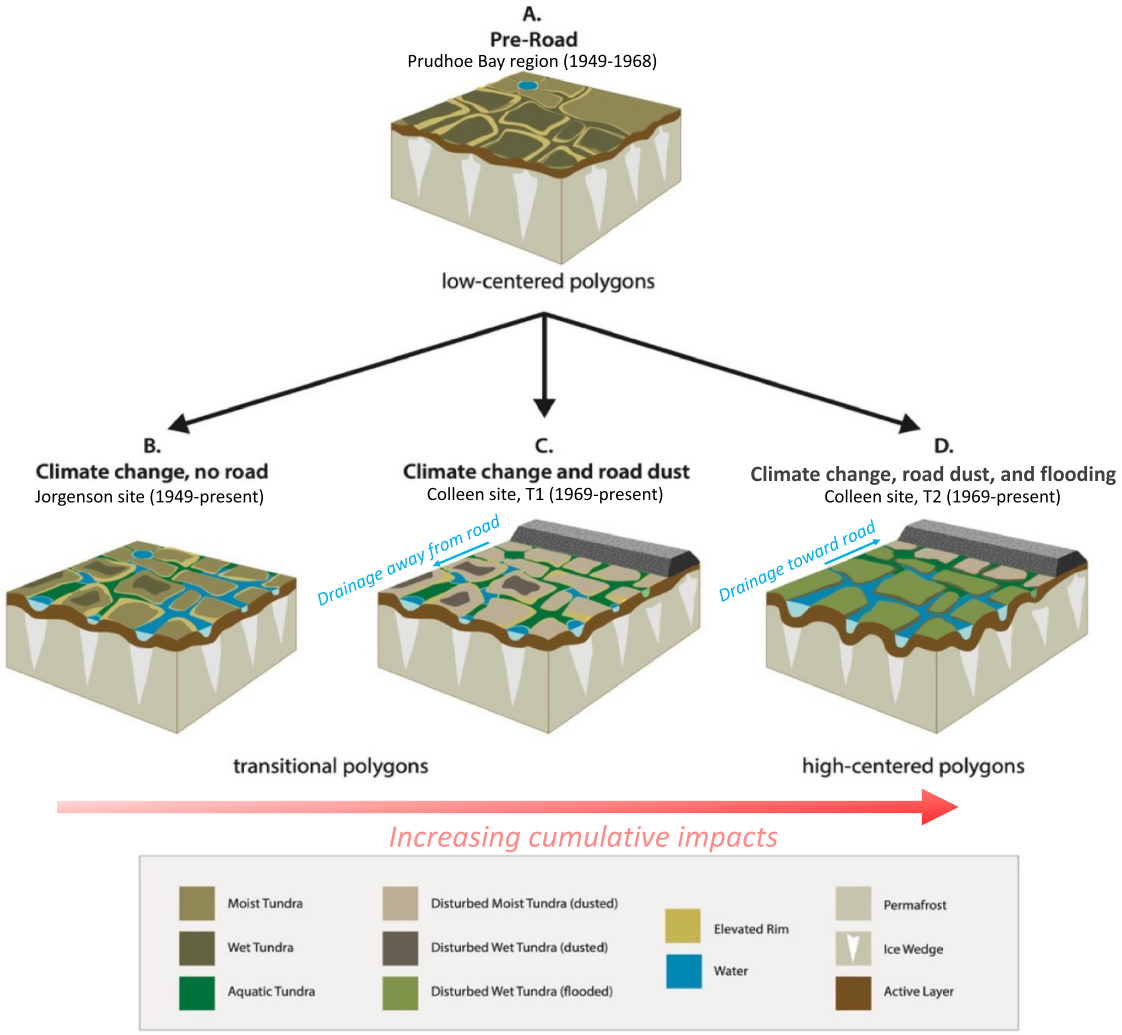

summarized in Jorgenson et al. (2015*a*) and (Kanevskiy et al. 2017, 2022).

At the Colleen site, 200-m transects were surveyed in 2014 perpendicular to both sides of the road to analyze impacts to landforms and vegetation in ice-wedge polygon centers and troughs in relationship to distance from the road (Fig. 3). Pin flags were placed at 1-m intervals from 1 m to 100 m and at 5-m intervals from 100 m to 200 m. Vertical 150-cm tall polyvinyl chloride (PVC) posts were placed at 5 m, 10 m, 25 m, 50 m, 100 m, and 200 m to mark the position of the transect for winter surveys. Elevations at each pin flag were determined using a Topcon® RTK GPS HyPer Lite + GPS surveying system. At each pin flag, we recorded the elevation, polygon microrelief feature (center, rim, trough, frost boil), dust-layer thickness (Varomorus® tubular soil sampler), leaf-area index (LAI, measured with an AccuPAR® LP-80, PAR/LAI Ceptometer), height of the vegetation, water depth and snow depth (measured with a meter stick), thaw depth (measured with a 1-m steel thaw probe), and vegetation type (Table S2.1).

To compare the microtopography of the CS and JS transects, we calculated elevation differences between centers and troughs of 11 ice-wedge polygons along the JS transect using historical 2013 transect elevation data (Jorgenson et al. 2015*a*) and compared the results with 2014 elevation data from nine polygons along CS T1 and nine polygons along CS T2 (Fig. S2.6). Thaw-depth, water-depth, and vegetation-distribution data were also collected at 1-m intervals from 0 m to 250 m along the JS transect in mid-August 2020 and compared with comparable data from the CS T1 and T2 transects measured a few days earlier.

Plot-based vegetation studies

The goals of the plot-based studies were to (1) examine trends in key environmental and vegetation variables within

plant communities of ice-wedge polygon centers and troughs along a gradient of distance from the road; (2) compare the species composition and environments in disturbed CS (2014) plots and comparable undisturbed plots sampled in the 1970s.

Field methods

We sampled 1 × 1-m permanent vegetation plots placed in polygon centers and troughs near transects T1 and T2 at 5 m, 10 m, 25 m, 50 m, 100 m, and 200 m from the road (Fig. 3). Two additional plots (plot numbers 14-4 and 14-5, not shown in Fig. 3) were placed in polygon centers approximately 385 m from the road along an extension of T1. Species cover of vascular plants, bryophytes (mosses and liverworts), and lichens was estimated using Braun-Blanquet cover abundance classes (Westhoff and Van der Maarel 1978). Environmental variables included ground-surface temperature (Maxim iButton® temperature loggers), thaw depth and water depth (8/7–10/2014), snow depth (3/27–30/2018), dust-layer thickness, soil organic matter in the top organic horizon (loss on ignition method), vegetation type (Table S2.1), (LAI, AccuPAR® LP-80, PAR/LAI Ceptometer), and visual estimates of percentage cover of plant growth forms (shrubs, graminoids, mosses, lichens). Soil pits were dug adjacent to the plots; soil plugs with dimensions approximately 15 × 15 cm in area and approximately 40 cm long were removed from the pit for description and collection of soil samples (Fig. S2.2c). Details of the plot and transect surveys are in two data reports (Walker et al. 2015, 2018).

Data management

Two vegetation plot datasets that are stored in the Alaska Arctic Vegetation Archive (AVA-AK, *https://arcticatlas.geobotany.org/catalog/group/plot-archive*) were used for the study: (1) 23 Prudhoe Bay plots sampled in 1975–1976 (Walker 2016); and (2) 26 CS plots sampled in 2014 (Walker 2017). The combined dataset contained 49 plots, 120 species, and 11 environmental variables (Supplemental file S3). The vegetation data management software TURBOVEG (Hennekens and Schaminée 2001) was used to store, select, and import vegetation data for analysis.

Initial classification

The plots sampled in the 1970s were assigned their original vegetation-type codes (Walker 1985, Types U3, U4, M2, M4, E1; Table S2.1). The CS plots sampled in 2014 were assigned tentative vegetation types using the same codes with the suffix 'd' added to indicate disturbed versions of the original vegetation (e.g., U3d, U4d, etc.). This subjective determination was based on habitat (moist, wet, and aquatic tundra) and the presence of common characteristic species in the 1970s vegetation units.

Cluster analysis of the combined 1970s and 2014 datasets

We used an agglomerative clustering approach to define floristically similar groups among the combined 1970s and 2014 datasets. The groupings were displayed as a dendrogram or tree diagram (McCune et al. 2002). The method hierarchically linked plots or groups of plots that had similar species composition into successively larger clusters. The 'crispness of classification' method (Botta-Duka´t et al. 2005) within the JUICE program (Tichy´ 2002; Tichy´ et al. 2011) helped to define the optimal number of clusters needed to achieve maximum separability of the derived clusters.

Species analyses

We compared the mean cover of plant growth forms (PGFs) in moist and wet vegetation types in the 1970s to those in the CS (2014) dataset. PGFs appearing in the species matrix (Table S3.1) were grouped into seven broader PGF categories (evergreen shrub, deciduous shrub, graminoid, forb, pleurocarpous moss, acrocarpous moss, and lichen). Cover-abundance scores for each species in the 2014 dataset were transformed to mean percentage cover values. Total cover was calculated for each PGF in each plot and then summarized for moist and wet tundra categories in the 1970s and 2014 datasets. Mean total cover of shrubs and key shrub species with cover >1% were summarized for moist and wet tundra in the 1970s and 2014 datasets.

A synoptic table (Table S2.2) was used to compare the growth-form and species composition of the disturbed vegetation units (2014) to comparable undisturbed vegetation units (1970s). We used the JUICE program (Tichý et al. 2011) to generate the synoptic table and lists of diagnostic species, constant species, and dominant species for each of the eight vegetation units (clusters from the cluster analysis). Diagnostic taxa are species with high fidelity to a given vegetation unit, i.e., they are regularly found in the given vegetation unit and are not regularly found in other units. Diagnostic species were determined using the Phi (Φ) coefficient (Chytrý et al. 2002), a statistical measure of species fidelity to each unit. Constant taxa are species that occur frequently in a vegetation unit but are not necessarily diagnostic because they may also be frequent in other units. Dominant taxa are species with relatively high cover in each vegetation unit. We tallied the number of species that satisfied index thresholds for fidelity ($\Phi = 35$), frequency (40%), and cover (2%) and summarized the results in a bar graph. Lists of the diagnostic, constant, and dominant species for each cluster accompany Table S2.2.

Ordination

The ordination synthesized the relationships of plots and vegetation units to environmental and anthropogenic disturbance gradients. We used the nonmetric multidimensional scaling (NMDS) ordination method available in the PC-Ord® software package (McCune et al. 2002). The matrices of species data (Table S3.1) and environmental data (Table S3.2) from 49 plots (26 Colleen plots and 23 comparable plots sampled in the 1970s) were prepared according to PC-Ord protocols. The NMDS ordination organized the plots in a two-dimensional ordination space based on their floristic similarity using the Sørensen distance measure (Kruskal 1964). Plots with similar species composition appear near each other in the ordination, and plots with dissimilar composition are far apart. Each plot's coordinates along Axes 1 and 2 were then correlated with environmental data using Kendall's rank (τ, tau) correlation for nonparametric variables. The cutoff for

Fig. 7. Waterbody distribution, Colleen site, 1968–2018. (*a*) Maps of waterbody distribution by years of analysis, with % of waterbody cover on the T1 and T2 sides of the road. (*b*) Area of waterbodies: T1 (blue lines), T2 (red lines), and entire map (gray lines). (*b*) Percent of water cover; (*c*) mean waterbody size; and (*d*) number of waterbodies. The images are a subset of the full 42 image record (Supplemental file S1). The 1968 photo was taken before construction of the Spine Road, which is the light horizonal band through the center of the 1972–2018 photos. (Aerial photographs: Quantum Spatial Inc., Anchorage, AK, permission courtesy of the BP Alaska Prudhoe Bay Unit).

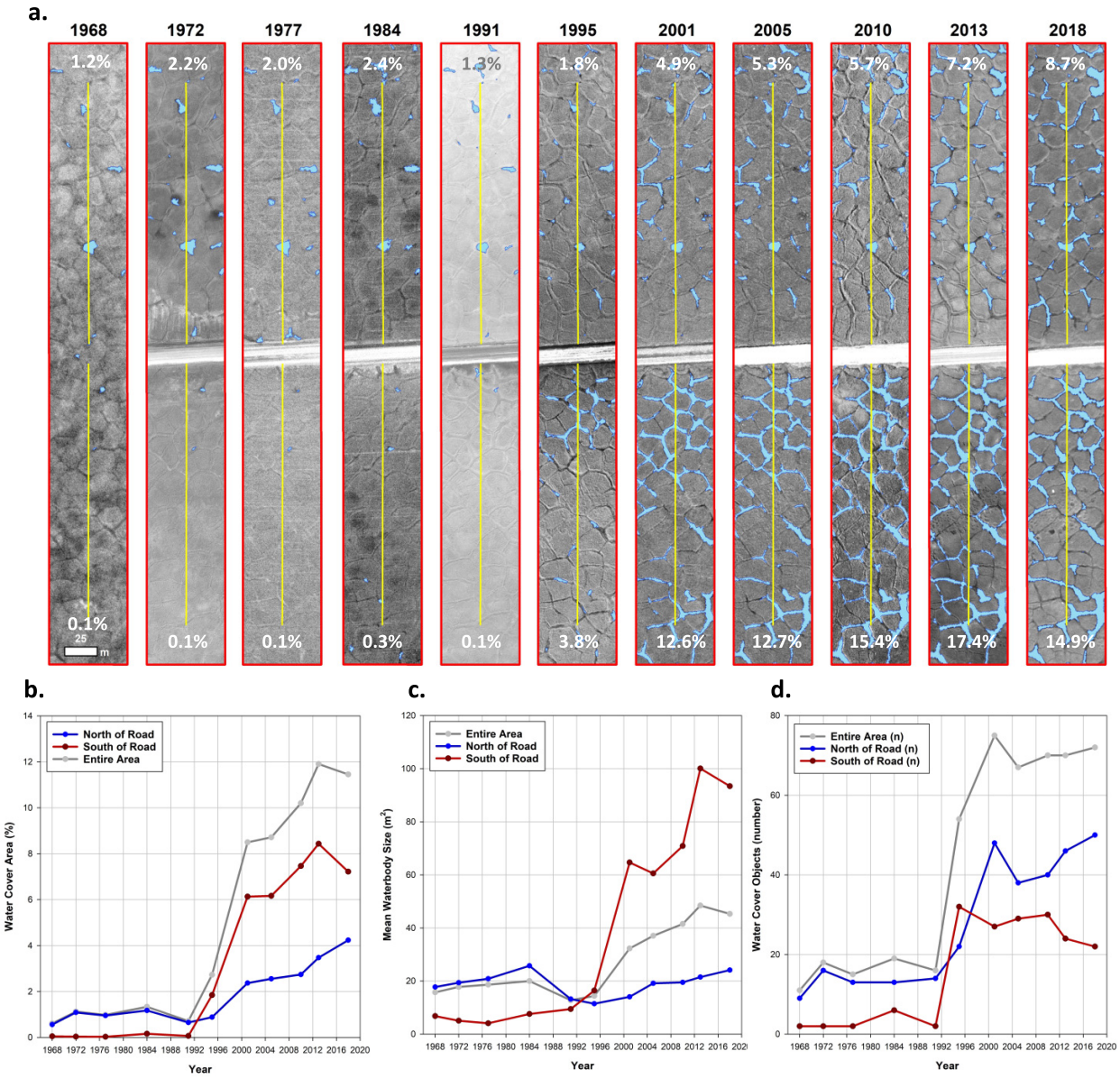

displaying significant environmental correlations along the axes was $\tau \geq 0.3$.

Results

Change in waterbody area

Jorgenson et al. (2015*a*) calculated the percentage area of waterbodies at the JS for four dates: 1949: 0.9%; 1988: 1.5%: 2004: 6.3%; and 2012: 7.5%—an approximately 7.5-fold increase in waterbodies since 1949, and an approximately 5-fold increase between 1988 and 2012.

The analysis of the CS ponds used images from 11 years (Fig. 7*a*). There was an overall 18.9-fold increase in total waterbody area for the entire CS site between 1968 and 2018 (Fig. 7*b*, gray lines). Most of the change occurred between 1991 and 2013—a 16.6-fold increase. The T1, nonflooded, side of the road had a 7.6-fold increase in pond area (Fig. 7*b*, blue line), similar to the 7.5-fold increase at the JS between 1949 and 2012. The T2, flooded side, had a 151.1-fold increase in waterbody area (Fig. 7*b*, red line). On the T2 side of the road, waterbodies became interconnected along polygon troughs, increasing the average area of individual waterbodies from less than 10 m^2 to 100 m^2, while the size of ponds on the T1 side of the road showed little change in mean size, averaging about 20 m^2 (Fig. 7*c*). The total number of waterbodies on the T1 side increased from 9 in 1968 to 50 in 2018, and

Fig. 8. Comparison of site factors and vegetation along Jorgenson site (JS) transect and Colleen transects (CS T1 and CS T2). (*a*) Distribution of ice-wedge-polygon trough-center elevation differences (cm) for *n* number of ice-wedge polygons along each transect determined from transect elevations collected at the JS transect in 2011 (Jorgenson et al. 2015*a*) and the CS transects in 2014 (Walker et al. 2015). (*b*) Thaw depth and water depth (15–17 August 2020), and snow depth (28 March 2016) in ice-wedge-polygon centers and troughs spaced at 1-m intervals along each transect. Colors are enhanced for the trough plots to help visualize the cumulative effects related to thaw depths, water depths, and snow depths in the deeper troughs of CS T2. (*c*) Distribution of barren, moist, wet, and aquatic vegetation types along JS in 2020; and CS T1 and CS T2 in 2014.

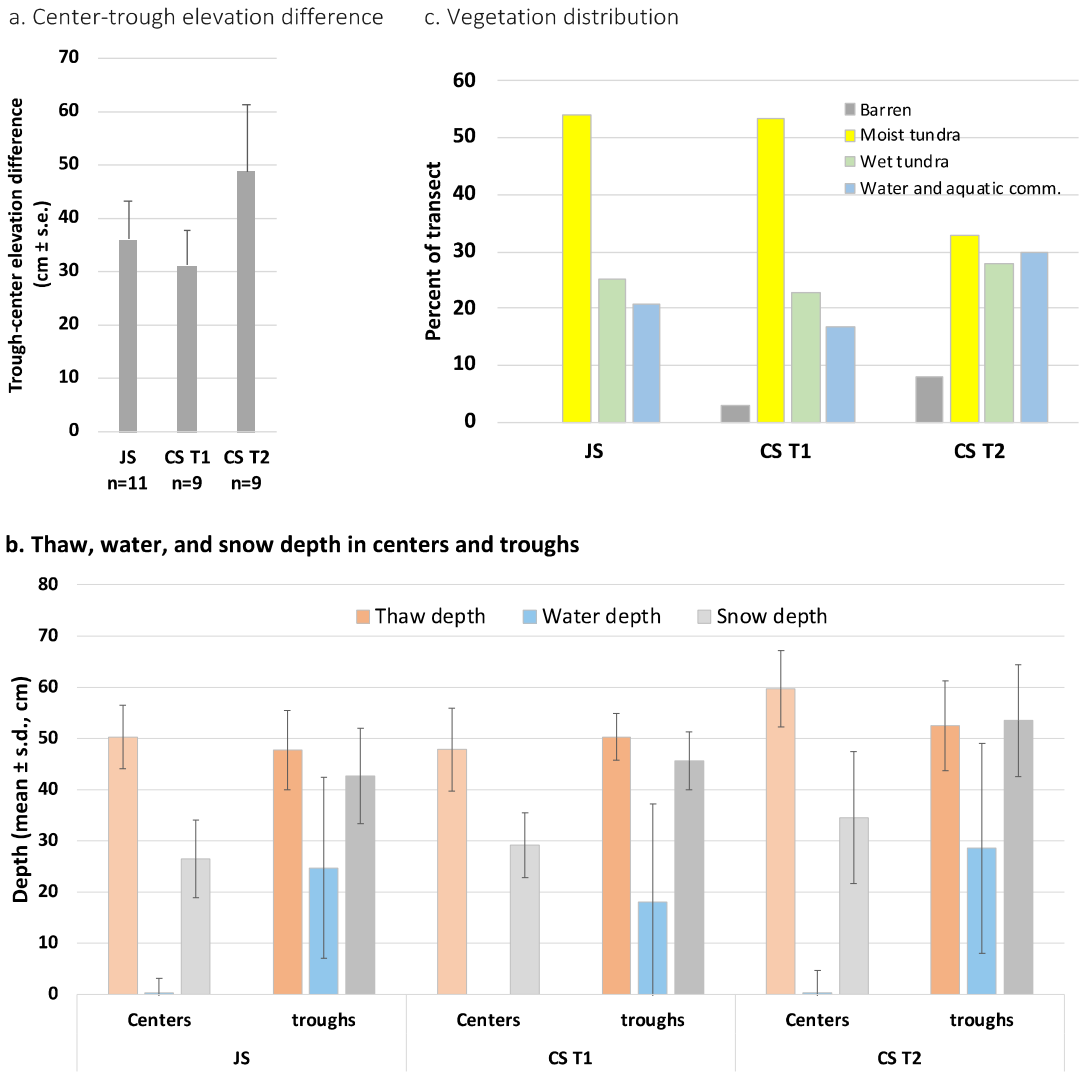

from 2 to only 22 on the T2 side because of the merging of ponds.

Variation in microtopography, thaw depths, water depths, snow depths, and vegetation distribution along the JS and CS transects

Polygon center-trough elevations differences were similar along the JS transect (36 ± 7.2 (s.e.) cm, measured in 2011) and CS-T1 transect (31.3 ± 6.4 cm, measured in 2014). CS-T2, had deeper and more variable trough depths (48.8 ± 12.4 cm, measured in 2014) (Fig. 8*a*). Snow depths and water depths were consequently also deepest and most variable in the CS-T2 polygon troughs (e, g., snow depths: JS, 41.9 ± 8.6 cm; CS-T1, 45.6 ± 0.3 cm; CS-T2, 48.8 ± 12.4 cm (Fig. 8*b*). The distribution of moist, wet, and water/aquatic tundra was similar along the JS and CS-T1 transects, while CS-T2 had much less moist tundra and much more water/aquatic tundra [cover moist/wet/aquatic tundra (%): JS: 54/25/21%; CS-T1: 54/23/17%; CS-T2: 33/28/30%, (Fig. 8*c*)].

Thaw depths, snow depths, and water depths were compared in relationship to patterned-ground features and roadside snow drifts along transects T1 and T2 (Fig. 9). A larger snowdrift occurred on the T2 (downwind) side of the road (maximum 85 cm deep and approximately 35 m long) compared with the T1 side (maximum 79 cm deep and approximately 15 m long). Water was confined to polygon troughs on

Fig. 9. Thaw depth and water depth (16 August 2016) and snow depth (28 March 2016) along CS T1 and T2. Variables were recorded at 1-m intervals and are overlaid on ice-wedge-polygon surface-form features (troughs, blue; low centers, green; flat and high centers, tan; and rims, orange). Snow drifts extended to approximately 10 m from the road along Transect T1 (predominant windward side of the road) and approximately 25 m from the road along T2 (predominant leeward side).

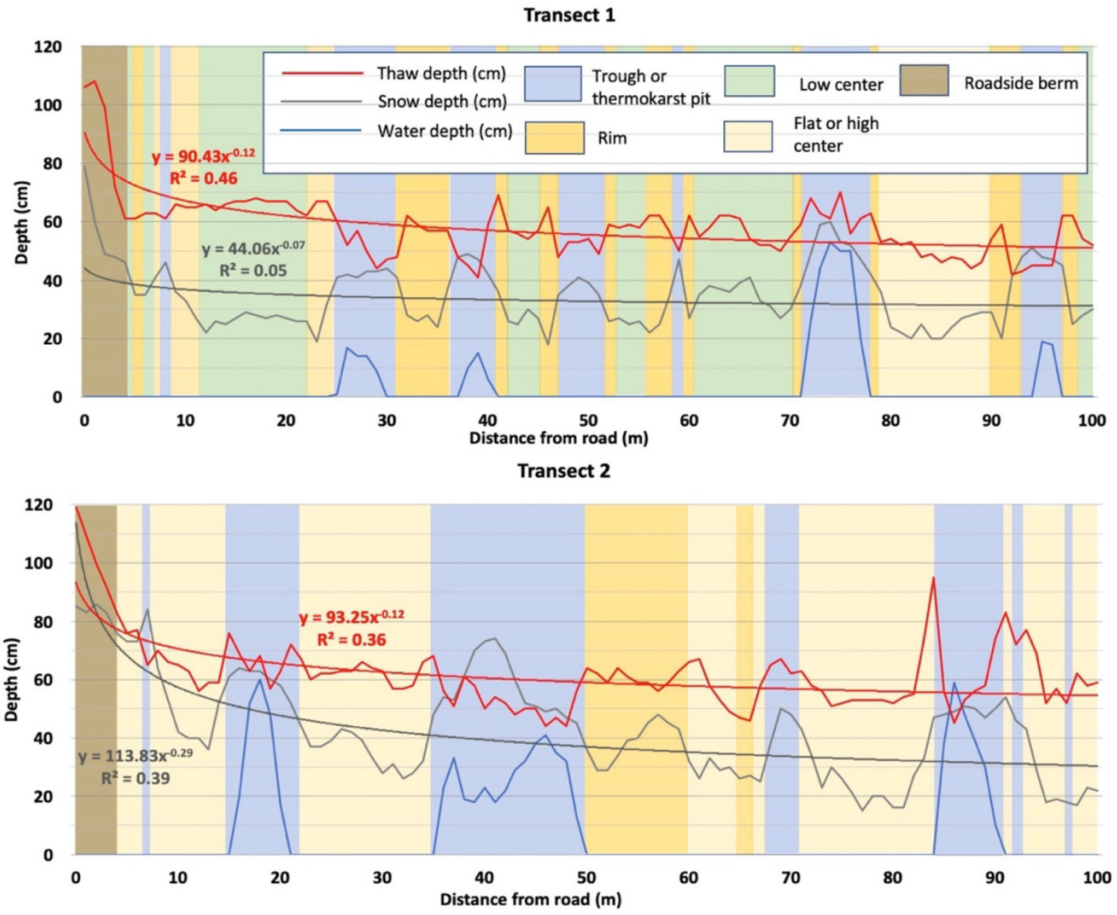

both sides of the road at the time of measurement (16 August 2016). Water depths in troughs ranged between 1 and 53 cm (mean ± sd = 20 ± 16 cm) on the T1 side, and between 10 and 60 cm (mean = 32 ± 14 cm) on the T2 side. Deeper summer thaw (up to 108 cm deep on the T1 side and up to 119 cm deep on the T2 side) occurred near the road in areas with snowdrifts. At greater distances from the road, snow depths were consistently deeper in polygon troughs compared with the centers, but thaw depths were often shallower in troughs because of the close proximity of underlying ice-wedges to the soil surface (Fig. 9).

Differences in key environmental and vegetation factors with distance from the road

A summary of the values of key environmental and vegetation variables measured in center and trough plots along Transects T1 and T2 are in Table S2.4 and Fig. S2.5. Best-fitting regressions of environmental and vegetation variables versus distance from the road are in Fig. 10. Separate lines were plotted for each variable for the center plots (orange dots in Fig. 10) and trough plots (blue dots). Best-fitting regression lines were shown if the coefficient of determination (R^2) was greater than 0.5. Many of the best-fitting equations were logarithmic as might be expected for variables that vary with wind distribution, such as road dust (Fig. 10*a*) and snow (Fig. 10*e*). Dust-layer thickness declined logarithmically with distance in polygon troughs on the T1 side of the road and logarithmically in both troughs and centers on the T2 side of the road ($R^2 > 0.89$) and linearly ($R^2 = 0.83$) in polygon centers on the T1 side. The logarithmic decreases in dust-layer thickness were reflected in the logarithmic increases of the percentage of soil organic matter in the surface soil organic horizons on both sides of the road ($R^2 > 0.84$, Fig. 10*b*) and the increases in moss cover with distance from the road on the T1 (unflooded) side of the road ($R^2 > 0.69$, Fig. 10*g*). Snow depth declined logarithmically with distance from the road in polygon centers on both sides of the road ($R^2 > 0.74$, Fig. 10*e*) and was likely largely responsible for the logarithmic declines in thaw depths due to warmer winter soil temperatures beneath the snowdrifts in polygon centers on both sides of the ($R^2 > 0.72$, Fig. 10*c*). The logarithmic trends were strongest on the

Fig. 10. Soil and vegetation factor trends in polygon centers and trough plots versus distance from road along transects T1 and T2. (*a*) Dust-layer thickness (cm); (*b*) organic matter, top O horizon (%); (*c*) thaw depth (cm, 8/27–30/2014); (*d*) mean annual soil surface temperature (°C, 2014–2015); (*e*) snow depth (cm, 3/28/2016); (*f*) S=species richness (nr. species/1-m^2 plot); (*g*) moss cover (%); (*h*) leaf-area index (m^2/m^2). Best-fitting regression lines with $R^2 \geq 0.5$ are displayed for centers (orange) and troughs (blue).

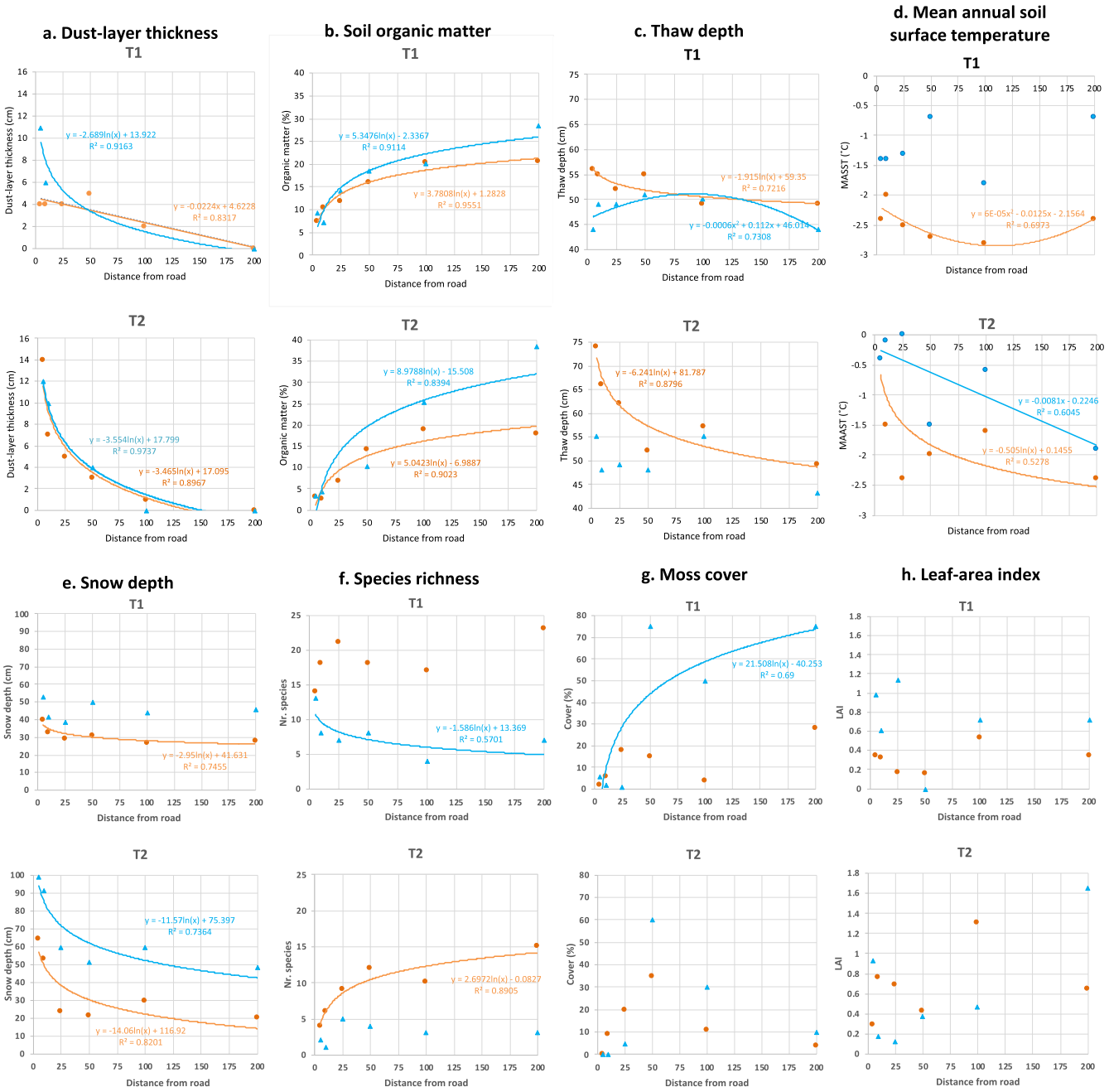

T2 side of the road, which is the predominantly downwind side. A few variables had best-fitting linear declines with distance from the road, for example, dust-layer thickness on the T1 side of the road ($R^2 = 0.83$) and mean annual soil-surface temperature on the T2 side of the road ($R^2 = 0.60$). Thaw depth in polygon troughs inexplicably peaked in the center of the T1 transect, and MASST in polygon centers dipped in the middle of the transect along T1 (best-fitting 2nd-order polynomial trends, $R^2 > 0.69$). Several, mainly vegetation-related variables, including leaf-area index (LAI), graminoid cover, and shrub cover showed no clear trends with distance from the road, although LAI was much greater on the T2 (flooded) side (mean LAI ± s.e.: T1, 0.51 ± 0.03; T2, 0.66 ± 0.04) and was over twice as high on the flooded T2 polygon centers (T1 centers, 0.32 ± 0.03; T2 centers, 0.69 ± 0.07) because of the lush growth of sedges.

Comparison of vegetation plots sampled in 2014 and comparable plots sampled in the 1970s

Vegetation classification

The cluster-analysis of the combined CS (2014) and Prudhoe (1970s) datasets resulted in eight vegetation units (clusters 1a–6a) and two outlier plots (T1-050-T and T2-005-C) (Fig. 11). Plot numbers were colored according to the legend below the dendrogram, based on the initial vegetation types assigned to plots before the cluster analysis. **Clusters 1a and 1b** contained all the undisturbed Prudhoe (1970s) moist tundra plots plus one relatively undisturbed CS (2014) plot (R14-4). **Cluster 2** contained all disturbed CS (2014) moist tundra plots. **Cluster 3** contained most of the undisturbed (1970s) wet tundra plots. **Clusters 4a and 4b** contained all the disturbed CS (2014) wet tundra plots; the T2 disturbed center plots were concentrated in Cluster 4a, and the T1 disturbed trough plots were concentrated in Cluster 4b. **Cluster 5** contained two CS (2014) and 3 Prudhoe (1970s) shallow-water aquatic plots. **Cluster 6a** contained a mix of 4 CS (2014) and 2 Prudhoe (1970s) deeper water aquatic plots. **Cluster 6b and cluster 4c** contained single outlier plots that were dissimilar to plots in all other clusters.

Spatial analysis of vegetation change

Comparisons of the 1972 and 2013 vegetation maps (Fig. 12) reveal the spatial transformations of the tundra on both sides of the road caused by a combination of climate change and the presence of the road. In 1972, the tundra on both sides of the road, except for an area of gravel spray adjacent to the road, was still like tundra in earlier photographs taken in 1949 and 1968, prior to construction of the road (Fig. S1.1). Low-centered polygons covered both sides of the road, and there was a mix of patches dominated by moist tundra (39.5%) and wet tundra (54.5%), with scattered small thermokarst ponds (2.3% aquatic tundra and water). By 2013, the damming effect of the road and the subsidence of the polygon troughs had converted most of the wet low polygon centers to transitional polygons with dominantly moist tundra in the polygon centers (72%) on the relatively well-drained T1 side of the road and to dominantly wet tundra (76%) on the flooded T2 side. Both sides had much more area of thermokarst ponds in 2013 (5.3% on the T1 side and 11.8% on the T2 side).

Growth-form and species differences

The disturbed CS (2014) moist tundra plots had 29% of the 1970s' cover of evergreen shrubs, and 5.2 times the cover of deciduous shrubs, about the same (35%) cover of graminoids, half the forb cover, and 38% of the pleurocarpous moss cover (Fig. 13*a*). Lichen cover in moist tundra sampled in the 1970s averaged 4.9% cover, compared with 0% cover in 2014.

Wet tundra in 2014 had 6.2 times the deciduous shrub cover of comparable plots sampled in the 1970s, 1.7 times the graminoid cover, 33% of the forb cover, 26% of the pleurocarpous moss cover, and 25% of the acrocarpous moss cover.

The evergreen prostrate dwarf shrub *Dryas integrifolia* Vahl (DRYINT) was most common in the undisturbed (1970s) moist tundra plots, whereas deciduous prostrate and erect willows *Salix arctica* (SALARC), *Salix ovalifolia* Pallas (SALOVA), *Salix reticulata* Trautv. (SALRET), and *Salix richardsonii* L. (SALRIC) were more common in the disturbed (2014) moist and wet tundra plots (Fig. 13*b*).

Many diagnostic species typically found in undisturbed moist and wet tundra sampled in the 1970s samples were missing or rare in the disturbed 2014 samples (Table S2.2, Fig. 13*c*). For example, 32 common moist-tundra diagnostic species in clusters 1a and 1b [undisturbed (1970s) moist tundra] are missing or rare in cluster 2 [disturbed (2014) moist tundra] (e.g., forbs: *Cardamine digitata* Richardson, *Draba alpina* L., *Hulteniella integrifolia* (Richardson) Tzelev, *Minuartia arctica* (Steven ex Ser.) Graebn., *Papaver macounii* Greene, *Pedicularis lanata* Cham. & Schtdl., *Saxifraga oppositifolia* L.,*Tephroseris frigida* (Richardson) Holub; mosses: *Abietinella abietina* (Hedw.) M. Fleisch., *Campylium bambergeri* (Schimp.) Hedenäs, Schlesak & D. Quandt (= *Hypnum bambergeri* Schimp.), *Pseudostereodon procerrimus* (Molendo) M. Fleisch. (= *Hypnum procerrimum* Molendo), *Oncophorus wahlenbergii* (Brid.), *Sanionia uncinata* (Hedw.) Loeske, and *Tomentypnum nitens* (Hedw.) Loeske; and lichens: *Cetraria islandica* (L.) Ach., *Dactylina arctica* (Hook. F.) Nyl., *Cetraria cucullata* (Bellardi) Ach., *Lecanora epibryon* (Ach.) Ach., *Masonhalea richardsonii* (Hook.) Kärnefelt, *Peltigera canina* (L.) Willd., and *Thamnolia subuliformis* (Ehrenb.) W.L. Culb.).

Change along environmental gradients

The ordination analysis (Fig. 14*a*) portrayed the separation of disturbed plots (2014, black circles) and comparable undisturbed plots (1970s, open squares) along environmental gradients based on their floristic similarity. Axes 1 and 2 captured 77% of the variance in species composition across all plots. Axis 1 was interpreted as a complex soil moisture/species richness/snow/shrub cover/lichen cover/pH gradient [tau coefficients: site moisture ($\tau = 0.69$), shrub cover ($\tau = -0.67$), water cover ($\tau = 0.64$), species richness ($\tau = 0.61$), snow regime ($\tau = 0.60$), water depth (0.57), lichen cover ($\tau = -0.43$), and soil pH ($\tau = -0.33$)]. Axis 2 was interpreted as a complex moss-cover/thaw-depth/lichen-cover/dust-layer disturbance gradient [tau coefficients: moss cover ($\tau = -0.53$), thaw depth ($\tau = 0.46$), lichen cover ($\tau = -0.44$), and dust-layer thickness ($\tau = 0.42$]. Figure 14*b* showed the plots and vegetation units (colored ellipses) in relationship to key environmental gradients as indicated by the group of orange environmental vectors in the center of the ordination space.

Discussion

Cumulative impacts along four trajectories of change

A tabular summary (Table S4.1) consolidates information regarding drivers and impacts of change to thermokarst

Fig. 11. Cluster analysis of CS (2014) and Prudhoe (1970s) plots. The plot numbers are color coded according to vegetation types assigned to each plot prior to the cluster analysis based on the vegetation types of Walker (1985, Table S2.1). The peak separability of the clusters was achieved with eight clusters and two outlier plots as shown by red dashed line. Brief descriptions of the numbered clusters are on the branches of the dendrogram.

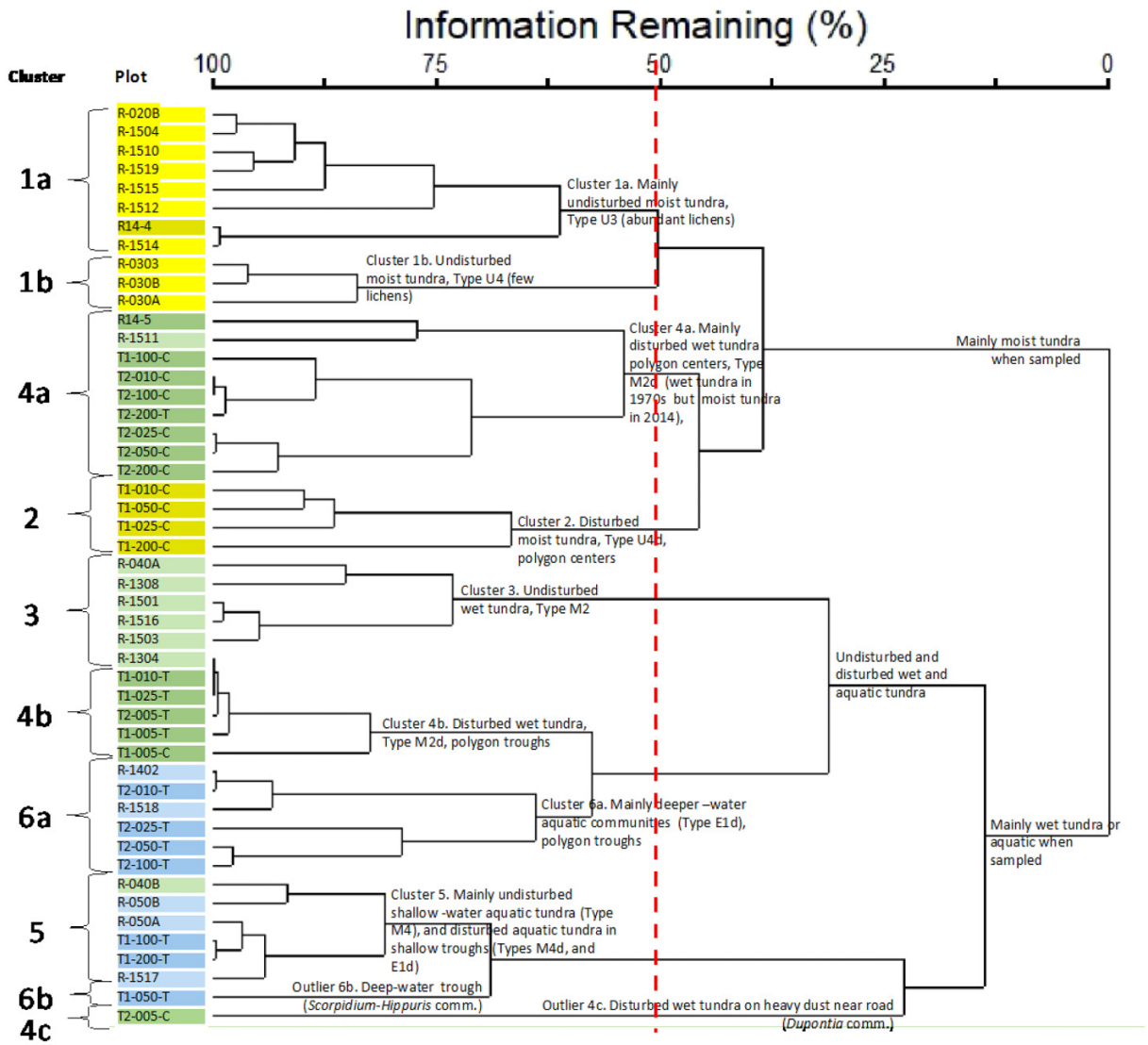

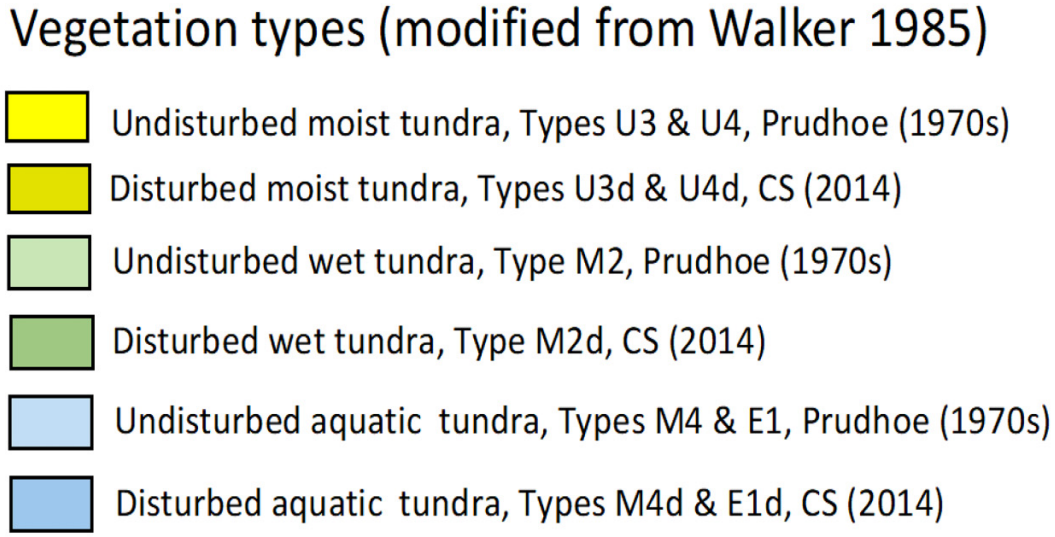

Fig. 12. Vegetation maps and analysis of the Colleen site in 1972 and 2013. The road was constructed in 1969 when the vegetation patterns were still like those prior to road construction. The maps illustrate the damming effect of the road, which prevents drainage of water from the T2 (SW) side of the road to the T1 (NE) side. Bar graphs show the distribution of broad vegetation types and water. (Derived from Raynolds et al. 2014*b*).

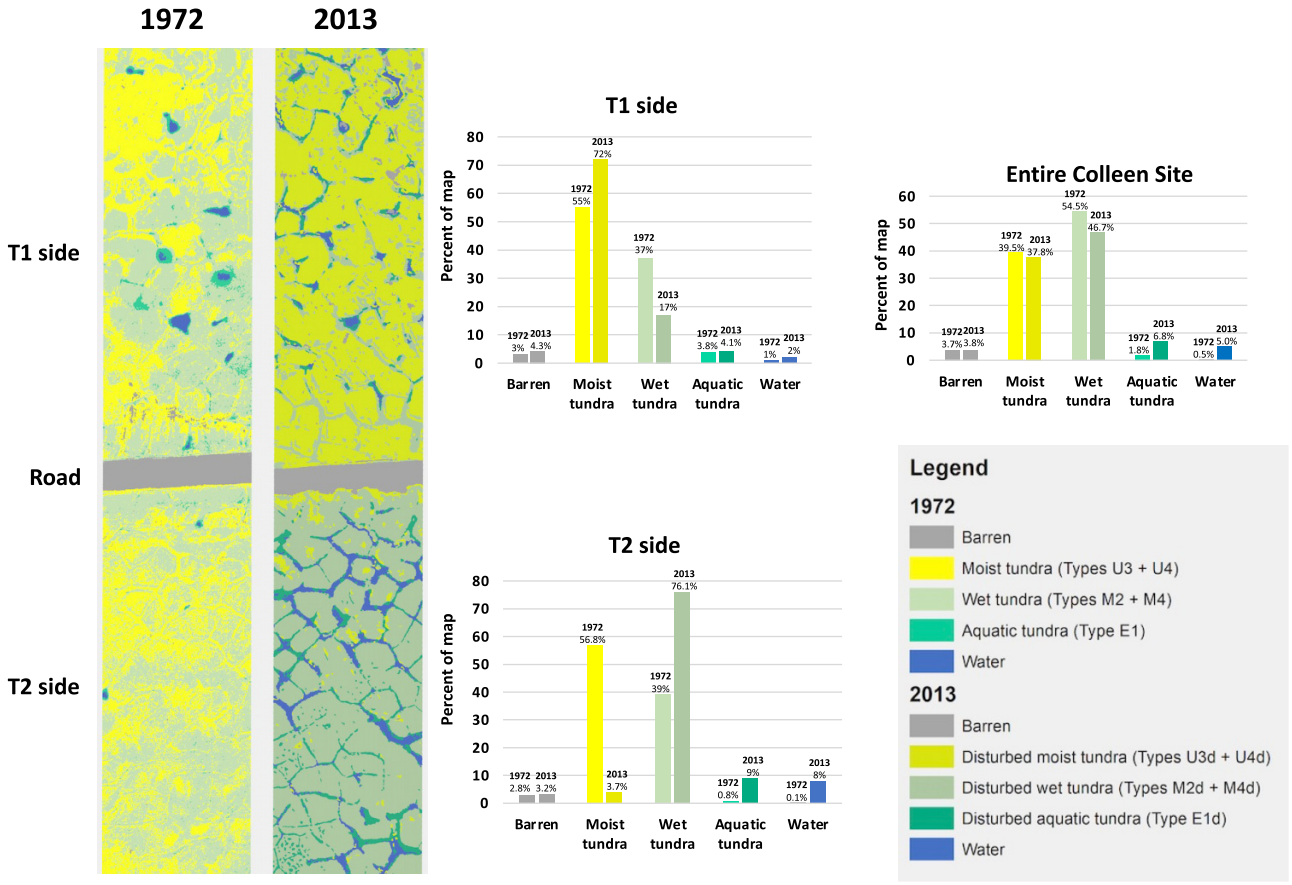

ponds, landforms and vegetation along each of the four trajectories of change in Fig. 6, with reference to key figures in this paper.

Trajectory A: prior to road construction (1949–1968)

Drivers of change

Trajectory A focused on the impacts of climate change to thermokarst ponds before oilfield development (1949–1968). In 1949, the Prudhoe Bay region was still a remote wilderness, and the primary drivers of change were natural landscape-evolution processes, including annual frost heave, successional processes related to pond expansion and drainage, and a small annual input of eolian dust from the Sagavanirktok river (Everett and Parkinson 1977; Walker 1985). There were no climate data available from the PBO prior to 1968, but data from Barrow indicate a relatively stable mean annual air temperature of -12.6° C ± 1.2° C and a slight cooling trend between 1949 and 1968. The upward trend of the MAAT started at Barrow in 1977 (US Climate Resilience Toolkit, *https://toolkit.climate.gov/image/1151*).

Cumulative impacts

There was little detectable change to the polygonal landforms or vegetation during 1949–1968. In 1949, most upland surfaces with near-surface ice wedges had a few thermokarst 'pits.' These small persistent ponds occurred mainly at the junction of ice-wedge-polygon troughs (Everett 1980c). For 20 years preceding development, the JS had only a few new small thermokarst ponds (Jorgenson et al. 2015a). A similar pattern occurred at the CS (Fig. S1.1). By 1968, there was less than 1% waterbody cover at the CS, concentrated in a few thermokarst ponds (Fig. 7).

Trajectory B: climate-related changes (1969–present)

Drivers of change

Climate change – Trajectory B focused on the climate-driven changes at the JS after discovery of the PBO. The unusually warm and wet summer of 1989 initiated a period of deep summer soil thaw and thermokarst pond development in north-central Alaska (Jorgenson et al. 2006). The trends in the mean annual temperature (MAAT), mean annual permafrost temperature (MAPT), and the mean active-layer thickness (ALT, the depth of annually thawed soil) all indicate a recent long

Fig. 13. Growth-form and species analysis. (*a*) Growth-form cover in groups of moist and wet undisturbed (1970s) and disturbed plots (2014). (*b*) Cover of shrub-species cover and total deciduous shrubs with greater than 1% cover in at least one of categories of moist- and wet-tundra plots, 1970s and 2014: DRYINT (*Dryas integrifolia*), SALARC (*Salix arctica*), SALOVA (*Salix ovalifolia*), SALRET (*Salix reticulata*), and SALRIC (*Salix richardsonii*). (*c*) Numbers of diagnostic, constant, and dominant species in each cluster (Table S2.2).

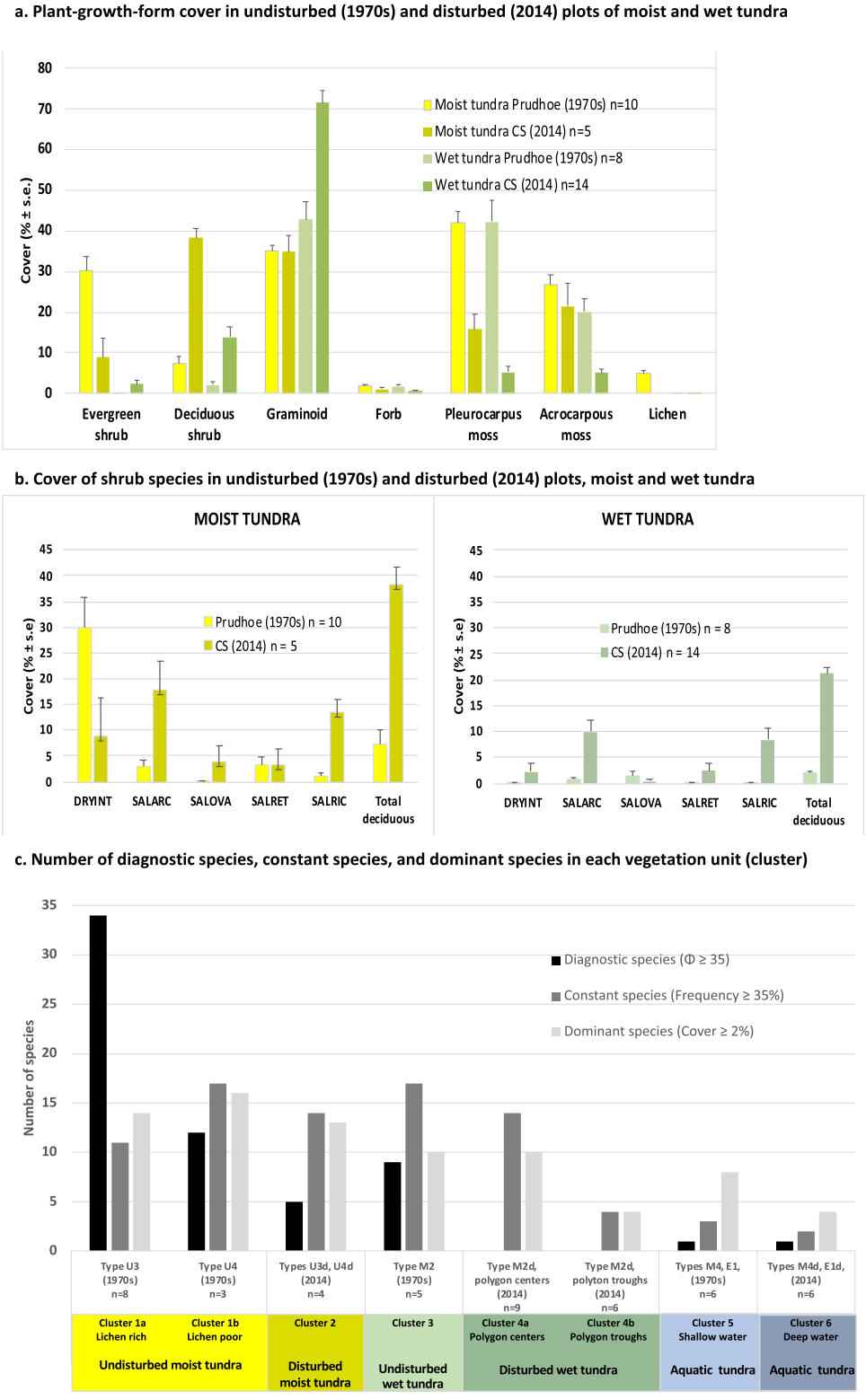

Fig. 14. Ordination of the disturbed CS (2014) and comparable undisturbed Prudhoe (1970s) plots. (*a*) NMS ordination of plots showing the distribution of undisturbed (1970s) plots (open squares), disturbed (2014) polygon-center plots (closed circles), and disturbed (2014) polygon-trough plots (closed inverted triangles). Labels are plot ID numbers: T1 and T2: transect number; middle three digits: distance from the road (m); T and C: trough, center. (*b*) Relationship of the groups of floristically similar plots (numbered ellipses, defined by cluster analysis) to environmental gradients depicted by orange vectors in the center of the ordination space showing direction and strength of correlations (R^2 cutoff > 0.2) with the indicated variables. Plot-symbol colors are according to vegetation types shown in the cluster analysis dendrogram (Fig. 9). The shapes and darkness of the symbols correspond to the year of sample (1970s, squares and lighter colors; 2014, circles and darker colors). Axes 1 and 2 are labeled with variables correlated with each axis. Correlation coefficients are in Table S2.3.

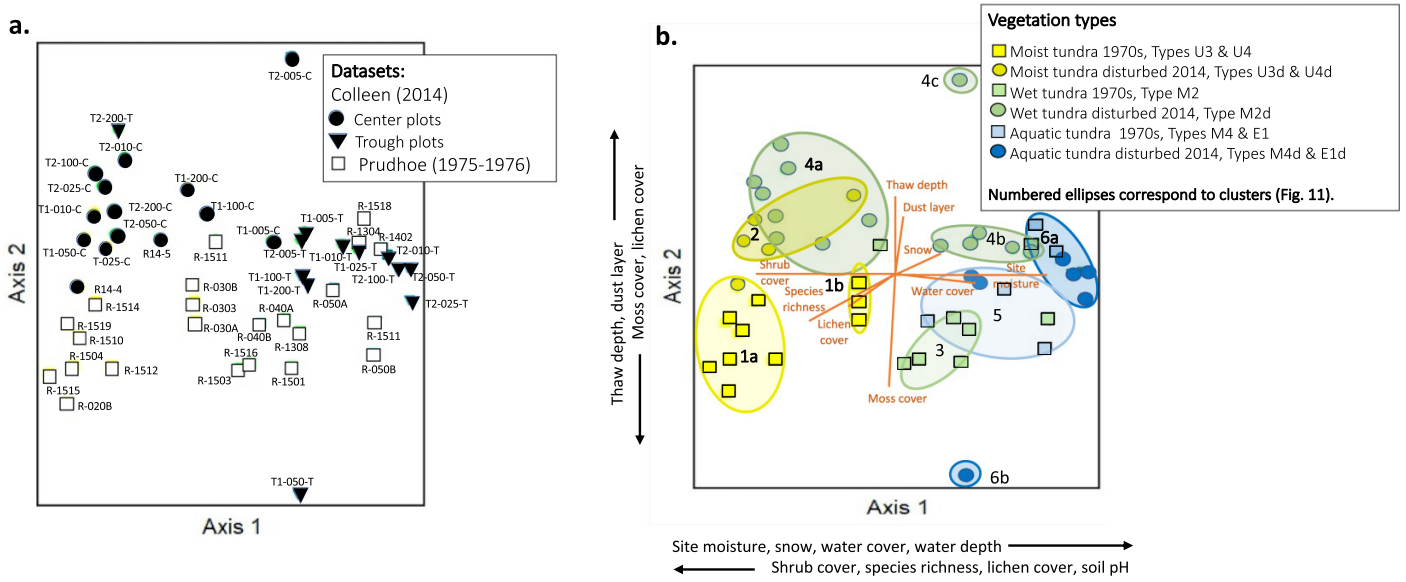

(1987–2019) strong warming trend in the PBO (Fig. 5*a*). The average summer warmth index (SWI, sum of the monthly mean temperature above 0°C, measured in thawing-degree months, °C mo) for the Deadhorse area between 1969 and 2019 was 19.6 ± 4.0 °C mo (mean ± sd) with a weak upward linear trend (R^2 = 0.21) (Fig. 5*b*). Years with the highest SWIs, 1989, 1998, and 2012 (Fig. 5*b*, dashed vertical red lines) corresponded to years with deep mean active-layer thickness at the Romanovsky Deadhorse site (ALT ≥ 68 cm, Fig. 5*a*).

No corresponding annual precipitation (AP) data were available for Deadhorse. AP and snowfall data from the Kuparuk Station, 47 km west of Deadhorse, show high annual variability (Fig. 5*c, d*). A recent abrupt increase in AP followed a gap in the record in 2012 and 2013. The snow record also has high variability and no trend for the length of the snow record (1983–2019).

Other drivers of change. – Other more subtle and unexamined contributors to change at the JS include seismic trails and air pollution. Vehicle trails from past seismic surveys can persist for many years and trigger thermokarst (Jorgenson et al. 2015*b*; Raynolds et al. 2020). 3D seismic trails are visible on aerial photographs of the JS and CS. In 2021, these old trails were difficult to detect on the ground, but occasional broken cottongrass tussocks (*Eriophorum vaginatum* L.) occurred on raised microsites, and some compressed vehicle tracks were observed. Our study also indicated a general reduction in lichen cover compared with observations in the 1970s (Fig. 13*c*) even at long distances from roads. Reduced lichen cover is most likely related to elevated regional road-dust (Walker and Everett 1987) and/or elevated air pollution levels (Richardson 1974; NRC 2003).

Cumulative impacts

The ice wedges at the JS are in varied states of degradation and stabilization. Jorgenson (2015*a*) proposed a quasi-cyclic ice-wedge trough evolution model consisting of five main stages: UD, undegraded ice wedges (narrow well vegetated troughs); DI, degradation initial (narrow troughs with shallow flooding); DA, degradation advanced (wide troughs, deeply flooded); SI, stabilization initial (wide troughs, shallow flooding); and SA, stabilization advanced (wide trough, water table below the soil surface). In some flooded troughs, ice wedges are continuing to degrade, while in others, eolian and eroded sediments and/or increased vegetation production protect the ice wedges from further degradation, permitting another cycle of ice-wedge growth (Kanevskiy et al. 2022).

Thermokarst also affects the water quality and microbiology in thermokarst-impacted water bodies (Vonk et al. 2015). At the JS, Koch et al. (2018) found that troughs in early stages of degradation received elevated nutrients that created higher ecosystem productivity. Deeper ponds had greater water-level fluctuations and hydrological gradients that promoted flow of water, solutes, and sediments toward the degraded troughs that eventually act to protect and stabilize the ice wedges (Kanevskiy et al. 2017). The altered distributions of water and energy created a more

heterogeneous landscape that strongly influenced a variety of ecosystem processes. including the emission of CO_2 and CH_4. Wickland et al. (2020) combined field measurements of trace gases with historical maps (1949–2018) of ice-wedge degradation and stabilization at the JS to assess how ice wedges and greenhouse gas exchange have changed over seven decades. They found that while increased plant production in the polygon troughs led to a 25% decrease in CO_2 emissions, methane emissions had increased by 42% due to the larger number of ponds. There was an overall 14% increase in seasonal CO_2-C equivalent to the atmosphere over 69 years.

Understanding the relationship of the various stages of ice-wedge degradation and stabilization to soil temperatures and thickness of protective layers above the ice wedges is a key to predicting future changes in the system (Kanevskiy et al. 2017, 2022). (Abolt et al. 2018, 2020) used a numerical model to investigate the effects of pond formation and surface drainage on polygon morphology and ground thermal properties at a nearby PBO site. The study found that deeper troughs led to snow accumulation and warmer winter soil temperatures; the coldest winter temperatures occurred in the polygon rims; larger rims promoted colder ice-wedge temperatures with more thermal cracking; and elimination of the rims through trough thermokarst erosion and trough subsidence led to high-centered polygon formation, profound changes in regional hydrology, and a much more heterogenous landscape. The impacts of aquatic plant communities on pond soil temperatures and the underlying ice wedges are currently being studied in ponds at and near the JS (Watson-Cook et al. 2021). The impact of vast areas of new thermokarst-ponds on other elements of the ecosystem, such as invertebrates, fish, waterbirds, mammals, and key subsistence species have not yet been investigated.

Trajectory C: climate- and dust-related changes (1969–present)

Drivers of change

Climate change – Both the JS and CS are within 4 km of the Deadhorse Station and 7.5 km of the Romanovsky Deadhorse site, so the climate trends were assumed to be the same for both sites (Fig. 5).

Road dust – Visually distinct surface dust layers (DLs) 1–14 cm thick occurred in all soil plugs at the CS taken from polygon centers within 100 m of the road on both sides of the road (Fig. 10*a*). Previous dust studies showed that summer winds at Deadhorse are predominantly from the northeast and distribute most road dust to the southwest side of roads (Everett 1980*a*). Compared with other sites along the Dalton Highway, the Prudhoe Bay site had the windiest conditions and exceptionally high volumes of dust. The volume of dust at 1000 m from the road in Everett's Deadhorse study site was 2 to 9 times greater than his other study sites at Franklin Bluffs, Sagwon, and Toolik, probably reflecting very high traffic volumes, the transport of dust to greater distances by higher wind velocities, and the contributions from numerous road sources in the PBO.

At the CS, dust affected the organic matter (OM) percentages in the uppermost soil horizons. OM varied from 2.5% to 38.5% of dry weight and had positive logarithmic increases with distance from the road in polygon centers and troughs on both sides of the road (Fig. 10*b*). Polygon troughs had somewhat higher OM percentages possibly due to higher OM production and less decomposition in the wetter colder soils of the troughs.

Other contributors to change – The road is elevated about 1.25 m above the tundra, which causes snow drifts and alters the natural drainage patterns on both sides of the road. Snowdrifts along heavily traveled roads collect large quantities of dust during the winter and spring, causing the roadside drifts to melt up to 2 weeks earlier than similar drifts along remote roads because of the relatively low albedos of the dust-covered snow (Benson et al. 1975). The snowdrifts also thermally insulate the soils, keeping the underlying tundra relatively warm during winter. The drifts also melt earlier than areas further from the roads, contributing to early-summer flooding, warmer early-summer soil temperatures, thicker active layers, and earlier vegetation greening near roads that attracts wildlife, including many waterbirds (Walker and Everett 1987; Truett et al. 1997). A variety of other roadside disturbances were generally greater within 25 m of the road, such as trails from off-road vehicles, a buried utility trench and impacts from road-maintenance activities, including gravel spray, snow removal, and dust-control chemicals (Fig. 15).

Cumulative impacts

Like the JS, there was little change to thermokarst patterns at the CS between 1949 and 1989 (Fig. S1.1). Between 1977 and 1987, some roadside thermokarst occurred in polygon troughs within 25 m of the road on the T1 side of the road but these vanished due to heavy road dust accumulating in the troughs. The somewhat smaller difference in center-trough elevations recorded along CS T1 compared with the JS (Fig. 9*a*) could also be due to dust accumulation in the polygon troughs, especially near the road. The summer of 1989 was exceptionally warm and wet with deep active layers. Thermokarst ponds formed in some polygon troughs along the T2 side of the road but not on the T1 side (Fig. S1.1, 1989). Several much cooler summers followed 1989, partially related to global cooling following the Mount Pinatubo eruption in June 1991 (Roback 2002). (Fig. 5*b*). 1991 was the coldest summer in the record. The summers of 1990–1993 were also drier than normal (Fig. 5*c*), and many of the flooded roadside polygon troughs that appeared in 1989 did not reappear in the 1990–1994 images. A wet and relatively warm summer in 1995 marked the beginning of a period of steady increase in thermokarst ponds on both sides of the road. The increase in thermokarst corresponded to a period of increasing mean annual thaw, mean annual permafrost temperature, and active layer thickness that was enhanced by the exceptionally warm summers in 1998 and 2012 and a large increase in summer precipitation during 2007–2019 (Fig. 5*c*).

Fig. 15. (*a*) Strip of 25-cm tall erect dwarf willows (*Salix richardsonii*) growing on NE (T1) side of the road along the line of a buried utility trench. The area at the base of the road embankment has high concentration of grasses. (*b*) Heavily dusted roadside area on the SW (leeward) side of the road. Numerous salt-tolerant species such as *Puccinellia andersonii* and *Puccinellia phryganodes* occur on the barren slope that has been created by the heavy dust. (*c*) Roadside willows (*Salix richardsonii*) up to 1 m tall growing near the Deadhorse Airport and the south side of Lake Colleen.

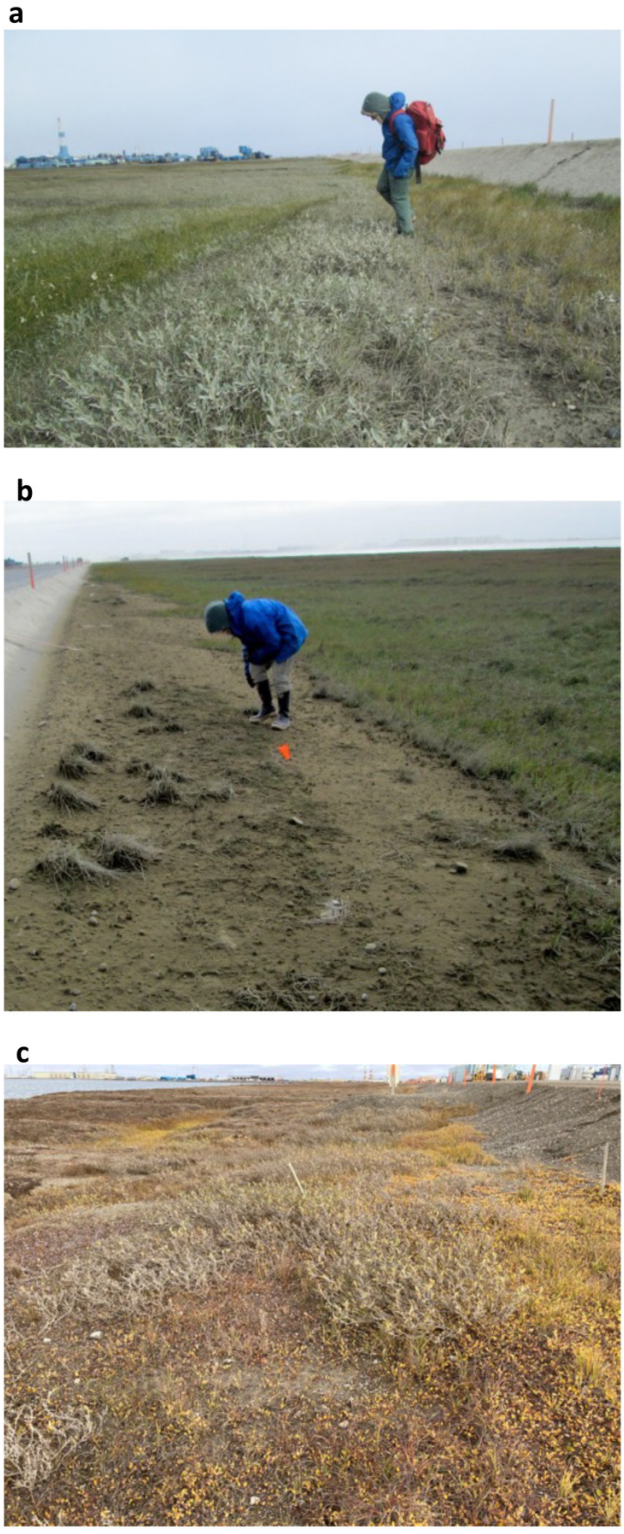

The cumulative impacts of road dust to the vegetation are discussed below ('Comparison of vegetation sampled in the 1970s and 2014').

Trajectory D. Climate-, dust- and flooding-related changes (1969–present)

Drivers of change

Climate change – The climate trends for CS-T2 are the same as indicated for trajectories B and C (Fig. 5).

Road dust – Surface dust layers (DLs) were thickest on the T2 (downwind) side of the road with 14 cm in one study plot at 5 m from the road (Fig. 10*a*) and exceeded 40 cm in some polygon troughs near to the T2 transect. DLs were generally thicker in polygon troughs compared with polygon centers at the same distance from the road and had negative logarithmic trends with distance from the road in both centers and troughs. The exceptionally thick dust layers near the SW side of the Spine Road completely buried pre-existing vegetation within a few meters of the road and created a well-drained gentle slope adjacent to the road that was colonized by a few ruderal salt-tolerant coastal and sand-dune species (Fig. 15*b*).

Flooding – By 2013, the SW side of the road (T2) had 2.4 times the cover of waterbodies (2402 m^2, 17.4% cover) as the T1 side (989 m^2, 7.2% cover) whereas prior to 1992, the T1 side had more waterbodies (Fig. 7). The flooding conditions and dominance of disturbed wet tundra on the T2 side of the road had three distinct interconnected causes—(1) ice-wedge degradation in troughs (discussed above), (2) blockage of natural drainage patterns by the Spine Road, and (3) variations in the water level in Lake Colleen. The Spine Road is one of several roads that surround Lake Colleen (Fig. 2*b*). The road is elevated approximately 1.25 m above the general tundra and acts as a dam preventing the cross drainage of flood waters toward the north. No culverts were placed along the 1.9 km straight section of road on the north side of the lake. During the Spring melt season and at other times of enhanced stream flow, water enters Lake Colleen through culverts on the west side of the lake, and the water level in the lake rises and backs up against the barrier of the road. During field observations in Aug 2014, a wave-cut strand line containing dead sedge leaves and stems uprooted by waterfowl was present approximately 45 cm above the level of ice-wedge-polygon centers along transect T2, and 75 cm above the water level in the troughs. The plant material was relatively fresh and was likely deposited during the melt season in 2014.

At the time of our field observations, water levels in all polygon troughs on the T2 side of the road were at the same elevation as the water level in Lake Colleen (Fig. S2.5), indicating that hydrological connections had developed between Lake Colleen and all the flooded troughs along T2. The aerial photo record indicates that these connections occurred at some point after 1995. Flooding enhanced the effects of climate change impacts to ice-wedge degradation. The greater microrelief contrasts along CS T2 (Fig. 9*a*) resulted in thicker active layers in polygon centers, and deeper thaw depths,

snow depths, and water depths in T2 polygon troughs compared with polygon troughs at CS T1 and JS (Fig. 9*b*).

Cumulative impacts

Road dust – Road-dust effects to the vegetation on the T2 side of the road were most severe within 10 m of the road (Fig. 15*b*). Several plants that are more typically found in salt marshes, beaches, and sand dunes near the coast occurred in heavily dusted plots near the road. The presence of the halophytes and coastal-dune species, for example, *Braya glabella* ssp. *purpurascens* (R. Br.) Cody, *Alopecurus magellanicus* Lam. *(= Alopecurus alpinus* ***Sm.****), Dupontia fisheri* R. Br., *Leymus arenarius* (L.) Hochst., *Puccinellia phryganodes* (Trin.) Scribn. & Merr., *P. andersonii* Swallen, and *Salix ovalifolia* Trautv., was likely related to salts used for dust control (Barnes and Connor 2014). At distances beyond about 10 m from the road, flooding conditions in the troughs and the tall sedge vegetation on polygon centers masked dust effects to the plants at the soil surface. The LAI, a unitless indicator of leaf surface area and plant biomass, was overall 34% higher in vegetation plots on the T2 side of the road compared with plots on the T1 side (mean LAI ± s.e.: T1, 0.55 ± 0.03; T2, 0.66 ± 0.04) and 2.1 times higher in polygon centers on the T2 side (T1 centers, 0.32 ± 0.03; T2 centers, 0.69 ± 0.07) (Table S2.4).

Flooding – The greater leaf area on the T2 side likely resulted from a combination of wetter early-summer soil moisture regimes, deeper thaw, higher rates of organic-matter decomposition, more nutrients from the dust, and high inputs of feces and decayed organic matter from the waterbirds that persistently graze the area. There is evidence that enhanced productivity and erosion of mineral material into the troughs is adding to the litter layer and helping to protect ice wedges from further thaw (Kanevskiy et al. 2017, 2022).

Vegetation changes since the 1970s

Differences in growth forms and diagnostic species

Substantially different moist and wet disturbed plant communities developed at the Colleen site by 2014 compared with similar undisturbed plant communities sampled in the 1970s (Table S2.2, Fig. 13). The disturbed (2014) moist tundra plots had less percentage cover of evergreen shrubs, forbs, mosses, and lichens and had more cover of deciduous shrubs (Fig. 13*a*). Many of the common diagnostic plant species that were present in the 1970s were not present in comparable 2014 plant communities. Thirty-two diagnostic species that were common in the undisturbed (1970s) plots did not occur in the disturbed CS (2014) samples, including several common basiphilous forbs, mosses, and lichens (Table S2.2, Fig. 13*c*). A few new ruderal salt-tolerant species were introduced in the disturbed habitats immediately adjacent to the road as described above (e.g., Fig. 15*b*).

The ordination shows the clear floristic separation of the disturbed (2014) and undisturbed (1970s) moist and wet plots along a complex natural site moisture/shrub/lichen/soil pH gradient (Axis 1), and a complex anthropogenic disturbance/thaw depth/moss and lichen cover gradient (Axis 2) (Fig. 14). The aquatic plots were not as clearly separated along the dust disturbance gradient but did show separation on the basis of water depth. The deeper ponds tended to be on the T2 (flooded) side of the road corresponding to the greater subsidence of ice-wedge polygon troughs in these plots.

Less cover of pleurocarpous mosses and lichens in disturbed plots

Moss cover was strongly impacted by dust impacts, and there was large contrast between the impacts to pleurocarpous mosses (highly branched mosses with many small leaves) and acrocarpous mosses (unbranched with erect habits and leaves coming off a central stem). The average pleurocarpous moss cover in the disturbed (2014) moist tundra plots was 38% of values in moist undisturbed (1970s) plots. Disturbed wet tundra plots had only 13% the cover of pleurocarpous mosses in comparable undisturbed plots. The highly branched structure of pleurocarpous mosses with many small leaves tend to trap dust and interfere with leaf-stomate function (Farmer 1993). Numerous common pleurocarpous mosses have also been shown to be sensitive to atmospheric nitrogen and sulfur deposition and other roadside pollutants (e.g., Ackermann et al. 2012). The more erect acrocarpous mosses more readily shed accumulations of dust and are often the pioneering mosses on bare soils near roads.

Lichens are early indicators of impacts to the vegetation because they are unprotected by a cuticle or stomata and are sensitive to high levels of SO_2, heavy metals, and road dust, which can build up to toxic levels (Richardson 1974; Seaward 1993). In 2014, no lichens were observed in any of the Colleen moist-tundra plots within 50 m of the road, and only three lichen species occurred with negligible cover in the plots at 385 m from the road (Table S3.1). The low cover near the roads is undoubtedly due to high road-dust loads that smother most cryptogams. Depletion of lichens at distances beyond 200 m from the road could be due to a combination of dust, industrial air pollution, and possibly repeated passage of off-road vehicles involved with seismic surveys.

More cover of deciduous shrubs in disturbed plots

The shrub information from the Colleen site (Fig. 13*b*) adds to current understanding of shrub expansion in northern Alaska and the Arctic (e.g., Sturm et al. 2001; Tape et al. 2006; Beck et al. 2011; Myers-Smith et al. 2011, 2015; Naito and Cairns 2015). The mean total deciduous shrub cover in the disturbed (2014) moist tundra plots at CS was 5.2 times more than the cover in similar plots sampled in the 1970s (Fig. 13*b*). Field photographs of plots sampled in 2014 showed abundant erect dwarf willows (*Salix richardsonii)* in moist tundra (e.g., Fig. S2.2a) versus a general lack of erect shrubs in photos taken at Prudhoe Bay in the 1970s (Walker 1985). The willow species *Salix arctica* and *S. richardsonii* had high cover both moist and wet disturbed plots. The greater cover of deciduous shrubs in the CS (2014) dataset could be due to a combination of responses to warmer summers and road-related disturbance. The occurrence of abundant erect dwarf shrubs

along the disturbed buried utility trench next to the road at the CS T1 (Fig. 15*a*) is a new phenomenon in the PBO and is an example of the combined influence of a warmer climate and soil disturbance. Highly disturbed soils in warmer Arctic areas are known to provide good habitat for rapid establishment of willows (Ebersole 1985; Walker et al. 1987*a*). Roadside willow-shrub communities are now common further south along warmer Arctic sections of the Trans-Alaska Pipeline (Dwight and Cairns 2018) and the Dalton Highway, but as of 2014, roadside willow shrublands were still uncommon in the colder coastal climate of the PBO except where there is also extensive surface disturbance as illustrated in Fig. 15*a*. Taller shrubs up to 1 m tall also occur in heavily disturbed roadside areas near the Deadhorse Airport (Fig. 15*c*). Studies of current vegetation more distant from roads are needed to determine if the high shrub-cover detected in the CS 2014 dataset is caused primarily by warmer regional summer temperatures or other disturbance-related factors.

More shrubs and graminoids in disturbed wet tundra

Disturbed (2014) wet tundra had 6.3 times as much deciduous-shrub cover as undisturbed wet tundra plots sampled in the 1970s (13.9% and 2.2%, respectively) and 1.6 times the graminoid cover (mainly sedges) (71.5% and 42.8%, respectively) (Fig. 13*a*). The high cover of shrubs in the 2014 wet tundra areas was unexpected because shrubs are generally not abundant in wet tundra habitats at Prudhoe Bay, but areas that were previously wet tundra areas in polygon centers were drained of excess flood waters by late summer on both sides of the road because of transformation of low-centered polygon to transitional and high centered polygons. The high wet-tundra graminoid cover and high LAI on the flooded T2 side of the road caused by early-summer flooding is likely contributing to stabilization of ice-wedge degradation (Kanevskiy et al. 2022).

Recommendations for future roads in areas with ice-rich permafrost

- Future cumulative impacts assessments for new roads and other forms of infrastructure need to consider the risk and likely consequences of climate-change and infrastructure-related impacts to permafrost, landforms, vegetation and ecosystems in areas with ice-rich permafrost.
- During the planning phase, multi-year baseline observations and descriptions of the geoecological and geotechnical conditions are needed, including details of the microtopography, distribution and structure of ice-rich permafrost, snow, and vegetation prior to any construction. Landscape sensitivity maps are needed for thermokarst risk assessment (e.g., Kanevskiy et al. 2017, 2022) and identification of the most at-risk areas.
- Cumulative impact assessments for activities during the early phases of development, such as leasing or seismic exploration, need to include the reasonably foreseeable direct and indirect cumulative impacts of the much more impactful exploration and development phases that would likely follow.
- A hierarchical perspective is needed to consider the cumulative consequences of climate change and land-use actions at local scales (e.g., this study), landscape and regional scales (e.g., Raynolds et al. 2014*a*, 2014*b*; Bergstedt et al. 2021), and global scales (e.g., Bartsch et al. 2020).
- Better methods are needed to decrease the effects of road dust, roadside snow drifts, and flooding to ice-rich permafrost and adjacent ecosystems. New remote sensing tools are improving monitoring permafrost terrain dynamics and infrastructure impacts of these factors. If construction occurs following a cumulative impact assessment, continue to monitor the effects of the infrastructure to inform future CIAs. Construction should be avoided altogether in landscapes with very high risk of ice-wedge degradation and high conservation and/or subsistence land-use value.

Conclusions

1. The explosive growth of the numbers and size of small ice-wedge thermokarst ponds during the past more than 30 years has transformed local drainage patterns. Studies of the consequences to hydrological systems, trace-gas fluxes, and thermal regimes of soils are being explored and modeled to some extent, but the full consequences of this major system change to other components of the system, such as aquatic plant communities, invertebrates, birds, and other fauna, still need to be documented.
2. The increase in erect-shrub cover since the 1970s near roads and at over 200 m from the roads is likely a consequence of a combination of the warming climate and road-related disturbances. These increases of shrubs in cold coastal landscapes are occurring more slowly than in inland areas.
3. Road dust has changed the distribution of common plant growth forms and the occurrence of many diagnostic species, especially small forbs, mosses, and lichens. Many dust-related impacts have logarithmic relationships to distance from the road and now extend to areas that are over 200 m from the road, especially on the downwind side of the road. Road dust has complex relationship with snow drifts ground temperatures, active-layer thickness, and ice-wedge degradation near roads.
4. Damming of natural drainage patterns by roads impacted the extent of flooding in polygon troughs, polygon microtopography, snow distribution, maximum thaw depths, and vegetation patterns. A wide variety of local factors, including wind and snow patterns, amount of ground ice, surficial geology, topography, soils, vegetation, and historical factors influence the trajectory of thermokarst, dust, and flooding. In this case, the proximity of Lake Colleen on the T2 side of the road greatly influenced the total area and interconnectivity of thermokarst features and the use of this area by waterfowl.
5. The use of historic baseline information, a variety of sampling strategies, and information from sites with different climate and infrastructure histories were useful for examining the long-term cumulative impacts to the landforms

and vegetation at the Colleen site but would be difficult to repeat where historic baseline information is lacking. Studies in other climates, geologic and topographic setting, and different types of road construction methods are needed to develop a broader understanding of the ecological consequences of building roads in areas with ice-rich permafrost.

6. Predicting the likelihood and extent of cumulative impacts of future development scenarios and climate change is currently very difficult. Much more work is needed to model the complex interactions of these factors. Improved strategies for detecting the presence of ice-rich permafrost (e.g., Witharana et al. 2021) and model-based approaches for predicting the consequences to the terrain and vegetation are being developed and could prove fruitful for future cumulative impact assessments (e.g., Abolt et al. 2018, 2020; Langer et al. 2016; Aas et al. 2019; Nitzbon et al. 2019, 2020; Schneider von Deimling et al. 2021). Broader application of newer remote-sensing tools, including very-high-resolution satellite data, unmanned-aerial-vehicle (UAV) photogrammetric surveys, structure-from-motion (SfM) photogrammetry, Airborne Light Detection and Ranging (LiDAR), and thermal imaging (e.g., van der Sluijs et al. 2018) will greatly improve landform and vegetation change detection at landscape and plot scales.

Acknowledgements

Primary financial support for this study came from the US National Science Foundation (grant numbers 1928237, 1263854) with contributions from the US National Aeronautics and the Space Administration (NASA grant numbers NNX14AD90G and NNX13AM20G), the Bureau of Ocean Energy Management, and US Geological Survey. Thanks to Jerry Brown, Pat Webber, and Kaye Everett (deceased) who had the foresight to conduct the early baseline ecological studies and mapping in the Prudhoe Bay region. Thanks to Georgy Matyshak for his contributions to field descriptions of the soils at the Colleen site. Thanks also to Bill Streever, BP Exploration (Alaska), Inc. (retired), who encouraged much of the field work presented here and obtained permission for use of the aerial photographs in Figs. 3*a*, 7, and Fig. S1.1 from the BP Alaska Prudhoe Bay Unit and Aeromap Inc. (now Quantum Spatial Inc.). Gary Kofinas contributed encouragement and ideas in earlier versions of the paper through the UAF EPSCoR program. This paper is an outcome of several workshops sponsored by the International Arctic Science Committee (IASC). Special thanks to two anonymous reviewers and Warwick Vincent who provided many helpful comments for inclusion of the manuscript in the T-MOSAiC Special Issue.

Article information

History dates

Received: 7 April 2021
Accepted: 20 December 2021
Accepted manuscript online: 2 March 2022
Version of record online: 26 July 2022

Notes

This paper is part of a Collection entitled “Terrestrial Geosystems, Ecosystems, and Human Systems in the Fast-Changing Arctic”.

Copyright

Author information

Author ORCIDs

Donald A. Walker http://orcid.org/0000-0001-9581-7811

Author contributions

DAW organized the effort at Lake Colleen and did much of the writing. MKR, ALB, JS, and AK provided ideas and writing for sections devoted to the vegetation description, analysis, and mapping. MZK and YS coordinated and conducted field research and wrote sections related to the permafrost component of the project. BMJ conducted the waterbody analysis and contributed text and ideas related to hydrology, remote sensing, and permafrost. VER and DN provided data, analyses, and insights regarding climate and permafrost temperatures. MB provided much of the remote sensing components of the project, surveyed the Colleen transect, and wrote early drafts of the field methods. MTJ provided data, ideas, and help with analysis of data from the Jorgenson site. JS, ALB, and EWC organized the vegetation archive and performed vegetation data analysis. HB provided dust analyses, ideas, and insights related to the dust distribution and snow. AL and RD provided insights, data, and interpretations of the hydrology aspects of the project. BC provided insights and key information regarding road construction and management of dust and hydrology-related cumulative impacts. JLP helped in all phases of the field work, data analyses, and manuscript preparation.

Supplementary materials

Supplementary data are available with the article at https://doi.org/10.1139/AS-2021-0014.

References

Aas, K.S., Martin, L., Nitzbon, J., Langer, M., Boike, J., Lee, H., Berntsen, T.K., and Westerman, S. 2019. Thaw processes in ice-rich permafrost landscapes represented with laterally coupled tiles in a land surface model. Cryosphere, **13**: 591–609. doi:10.5194/tc-13-591-2019

Abolt, C.J., Young, M.H., Atchley, A.L., and Harp, D.R. 2018. Microtopographic control on the ground thermal regime in ice wedge polygons. Cryosphere, **12**: 1957–1968. doi:10.5194/tc-12-1957-2018

Abolt, C.J., Young, M.H., Atchley, A.L., Harp, D.R., and Coon, E.T. 2020. Feedbacks between surface deformation and permafrost degradation in ice wedge polygons, Arctic Coastal Plain, Alaska. J. Geophys. Res.-Earth, **125**: e2019JF005349. doi:10.1029/2019JF005349

Ackerman, D.E., and Finlay, J.C. 2019. Road dust biases NDVI and alters edaphic properties in Alaskan arctic tundra. Sci. Rep.-UK, **9**: 207. Available from: https://www.nature.com/articles/s41598-018-36804-3.pdf?proof=t%29.

Ackermann, K., Zackrisson, O., Rousk, J., Jones, D.L., and DeLuca, T.H. 2012. N2 fixation in feather mosses is a sensitive indicator of N deposition in boreal forests. Ecosystems, **15**: 986–998. doi: 10.1007/s10021-012-9562-y.

Auerbach, N.A., Walker, M.D., and Walker, D.A. 1997. Effects of roadside disturbance on substrate and vegetation properties in arctic tundra. Ecol. Appl. **7**: 218–235. doi:10.1890/1051-0761(1997)007[0218:EORDOS]2.0.CO;2

BLM. 2019. Coastal plain oil and gas leasing program environmental impact statement. U.S. Department of Interior, Bureau of Land Management, 387pp. Available from: https://eplanning.blm.gov/public_projects/nepa/102555/20003762/250004418/Volume_1_ExecSummary_Ch1-3_References_Glossary.pdf.

Bartsch, A., Pointner, G., Ingeman-Nielsen, T., and Lu, W. 2020. Towards circumpolar mapping of Arctic settlements and infrastructure based on Sentinel-1 and Sentinel-2. Remote Sens. **12**(15): 2368. doi: 10.3390/rs12152368

Barnes, D., and Connor, B. 2014. Managing dust on unpaved roads and airports. Alaska University Transportation Center and Alaska Department of Transportation and Public Facilities, INE/AUTC 14.14, 84pp. Available from: http://hdl.handle.net/11122/7523

Beanlands, G., and Duinker, P. 1983. An ecological framework for environmental assessment in Canada. Federal Environmental Assessment Review Office, Hull, Quebec. pp. 1–127. Available from: https://www.researchgate.net/profile/Peter-Duinker/publication/236399538_An_Ecological_Framework_for_Environmental_Impact_Assessment_in_Canada/links/5919969d4585159b1a4b8060/An-Ecological-Framework-for-Environmental-Impact-Assessment-in-Canada.pdf

Beck, P.S.A., Horning, N., Goetz, S.J., Loranty, M.M., and Tape, K.D. 2011. Shrub cover on the North slope of Alaska: circa 2000 baseline map. Arct. Alpine Res. **43**: 355–363. doi:10.1657/1938-4246-43.3.355.

Benson, C., Holmgren, B., Timmer, R., Weller, G., and Parrish, S. 1975. Observations on the seasonal snow cover and radiation climate at Prudhoe Bay, Alaska during 1972. *In* Ecological investigations of the Tundra Biome at Prudhoe Bay, Alaska. *Edited by* J. Brown. Biological Papers of the University of Alaska, Fairbanks. Special Report 2. pp 12–50. Available from: https://www.arlis.org/docs/vol1/B/3035866.pdf.

Bergstedt, H., Jones, B., Walker, D., Pierce, J., Bartsch, A., and Pointner, G. 2021.Quantifying the spatial and temporal influence of infrastructure on seasonal snow melt timing and its influence on vegetation productivity and early season surface water cover in the Prudhoe Bay Oilfields. EGU General Assembly. **21**: 10296. Available from: https://meetingorganizer.copernicus.org/EGU21/EGU21-10296.html.

Botta-Duka´t, Z., Chytry´, M., and Ha´jkova´, P. 2005. Vegetation of lowland wet meadows along a climatic continentality gradient in Central Europe. Preslia. **77**: 89–111. Available from: https://ecolres.hu/sites/default/files/P051CBot.pdf.

J. Brown(ed.). 1975. Ecological investigations of the Tundra Biome in the Prudhoe Bay Region, Alaska. Biological Papers of the University of Alaska, Special Report 2, 240pp. Available from: https://www.arlis.org/docs/vol1/B/3035866.pdf.

Brown, J., and Berg, R. 1980. Environmental engineering and ecological baseline investigations along the Yukon River-Prudhoe Bay Haul Road. U.S. Army Cold Regions Research and Engineering Laboratory, Hanover, NH. 187pp. Available from: https://erdc-library.erdc.dren.mil/jspui/handle/11681/9550.

Buchhorn, M., Kanevskiy, M., Matyshak, G., et al. 2014. Effects of 45 years of heavy road traffic on permafrost and tundra along the Spine Road at Prudhoe Bay, Alaska. Presented at Arctic Change 2014. Ottawa, December 8-12. Abstract 339. Available from: https://www.geobotany.uaf.edu/library/posters/Buchhorn2014_OttawaAC2014_pos20141205.pdf.

CEQ (Council on Environmental Quality). 1997. Considering Cumulative Effects Under the National Environmental Policy Act. Council on Environmental Quality, Executive Office of the President, Washington, DC. Available from: https://ceq.doe.gov/docs/ceq-publications/ccenepa/exec.pdf.

Chytrý, M., Tichý, L., Holt, J., and Botta-Dukát, J. 2002. Determination of diagnostic species with statistical fidelity measures. J. Veg. Sci. **13**: 79–90. doi:10.1111/j.1654-1103.2002.tb02025.x.

Clark, R. 1994. Cumulative effects assessment: a tool for sustainable development. Impact Assess. **12**(3): 319–331. doi:10.1080/07349165.1994.9725869.

Connelly, R. 2011. Canadian and international EIA frameworks as they apply to cumulative effects. Environ. Impact Assess. Rev. **31**(5): 453–456. doi:10.1016/j.eiar.2011.01.007.

Connor, B., Goering, D.J. Kanevskiy, M., Trochim, E., Bjella, K., and McHattie, R.L. 2020. Roads and airfields constructed on permafrost: a synthesis of practice. Report No. 000S927. University of Alaska Fairbanks, Institute of Northern Engineering, Alaska Department of Transportation and Public Facilities, Fairbanks, Fairbanks AK. Available from: http://www.dot.state.ak.us/stwddes/research/assets/pdf/000S927.pdf.

DOI (Department of Interior). 2021. Interior Department suspends oil and gas leases in Arctic National Wildlife Refuge. Available from: https://www.doi.gov/pressreleases/interior-department-suspends-oil-and-gas-leases-arctic-national-wildlife-refuge.

Dwight, R.A., and Cairns, D.M. 2018. The Trans-Alaska Pipeline System facilitates shrub establishment in northern Alaska. Arctic. **71**: 249–258. doi: 10.14430/arctic4729

EC (European Commission). 1999. Study on the assessment of indirect and cumulative impacts as well as impact interactions. Cardiff, United Kingdom: European Commission, 189pp. Available from: http://aei.pitt.edu/40404/1/A4813.pdf.

Ebersole, J.J. 1985. Vegetation disturbance and recovery at the Oumalik Oil Well, Arctic Coastal Plain, Alaska. Ph.D. thesis, University of Colorado, Boulder. Available from: http://libraries.colorado.edu/record=b1700318~S3.

Everett, K.R. 1980a. Chapter 3. Distribution and properties of road dust along the northern portion of the haul road. *In* Environmental Engineering and Ecological Baseline Investigations along the Yukon River Prudhoe Bay Haul Road. *Edited by* J. Brown and R.L. Berg. Army Cold Regions Research and Engineering Laboratory, Hanover, NH. CRREL Report 80-19. pp. 101–128. Available from: https://hdl.handle.net/11681/9550.

Everett, K.R. 1980b. Geology and permafrost. *In* Geobotanical atlas of the Prudhoe Bay region, Alaska. *Edited by* D.A. Walker, K.R. Everett, P.J. Webber and J. Brown. U.S. Army Corps of Engineers, Cold Regions Research and Engineering Laboratory, Hanover, NH. pp 8–9. CRREL Report 80-14. Available from: http://acwc.sdp.sirsi.net/client/en_US/search/asset/1027400;jsessionid=6F5EF40051DE66DA706D4275CB11F7D1.enterprise-15000.

Everett, K.R. 1980c. Landforms. *In* Geobotanical atlas of the Prudhoe Bay region, Alaska. *Edited by* D.A. Walker, K.R. Everett, P.J. Webber and J. Brown. U.S. Army Corps of Engineers, Cold Regions Research and Engineering Laboratory, Hanover, NH. pp. 14–19. CRREL Report 80-14. Available from: http://acwc.sdp.sirsi.net/client/en_US/search/asset/1027400;jsessionid=6F5EF40051DE66DA706D4275CB11F7D1.enterprise-15000.

Everett, K.R. 1980d. Soils. *In* Geobotanical atlas of the Prudhoe Bay region, Alaska. *Edited by* D.A. Walker, K.R. Everett, P.J. Webber and J. Brown. U.S. Army Corps of Engineers, Cold Regions Research and Engineering Laboratory. Hanover, NH. pp. 20–22. CRREL Report 80-14. Available from: http://acwc.sdp.sirsi.net/client/en_US/search/asset/1027400;jsessionid=6F5EF40051DE66DA706D4275CB11F7D1.enterprise-15000

Everett, K.R., and Parkinson, R.J. 1977. Soil and landform associations, Prudhoe Bay area, Alaska. Arct. and Alpine Res. **9**: 1–19. Available from: https://www.jstor.org/stable/1550406?origin=&seq=1#metadata_info_tab_contents.

Everett, K.R., Webber, P.J., Walker, D.A., Parkinson, R.J., and Brown., J. 1978. A geoecological mapping scheme for Alaskan coast tundra. *In* Proceedings of the Third International Conference on Permafrost, **Vol 1**. Edmonton, National Research Council of Canada. pp. 360–365. Available from: https://www.arlis.org/docs/vol1/ICOP/6490307v1.pdf.

Everett, K.R., Walker, D.A., and Webber, P.J. 1980. Master map: Prudhoe Bay region, Alaska, area 2. *In* Geobotanical atlas of the Prudhoe Bay region, Alaska. *Edited by* D.A. Walker, K.R. Everett, P.J. Webber and J. Brown. U.S. Army Corps of Engineers, Cold Regions Research and Engineering Laboratory, Hanover, NH. pp. 61. CRREL Report 80-14. Available from: https://erdc-library.erdc.dren.mil/jspui/handle/11681/9008.

Farmer, A.M. 1993. The effects of dust on vegetation-a review. Environ. Pollut. **79**: 63–75. doi: 10.1016/0269-7491(93)90179-R

Farquharson, L.M., Romanovsky, V.E., Cable, W.L., Walker, D.A., Kokelj, S.V., and Nicolsky, D. 2019. Climate change drives widespread and rapid thermokarst development in very cold permafrost in the Canadian High Arctic. Geophys Res. Lett. **46**(12): 6681–9. doi: 10.1029/2019GL08218782187.

Ferrians, O.J.J., Kachadoorian, R., and Greene, G.W. 1969. Permafrost and related engineering problems in Alaska. U.S. Geological Survey Professional Paper 678, 37pp. Available from: https://pubs.usgs.gov/pp/0678/report.pdf.

Fraser, R.H., Kokelj, S.V., Lantz, T.C., McFarlane-Winchester, M., Olthof, I., and Lacelle, D. 2018. Climate sensitivity of high arctic permafrost terrain demonstrated by widespread ice-wedge thermokarst on Banks Island. Remote Sens.-Basel. **10**: 954. doi:10.3390/rs10060954.

Frost, G., Christopherson, T., Jorgenson, M., Macander, M.J., Walker, D., and Wells, A. 2018. Regional patterns and asynchronous onset of ice-wedge degradation since the mid-20th century in Arctic Alaska. Remote Sens.-Basel. **10**: 1312. doi: 10.3390/rs10081312

Gill, H.K., Lantz, T.C., O'Neill, B., and Kokelj, S.V. 2014. Cumulative impacts and feedbacks of a gravel road on shrub tundra ecosystems in the peel plateau, Northwest Territories, Canada. Arctic and Alpine Res. **46**: 947–961. doi: 10.1657/1938-4246-46.4.947.

Godin, E., Fortier, D., and Coulombe, S. 2014. Effects of thermo-erosion gullying on hydrologic flow networks, discharge and soil loss. Env. Res. Lett. **9**: 105010. doi:10.1088/1748-9326/9/10/105010.

Godin, E., Fortier, D., and Lévesque, E. 2016. Nonlinear thermal and moisture response of ice-wedge polygons to permafrost disturbance increases heterogeneity of high Arctic wetland. Biogeosciences. **13**: 1439–1452. doi:10.5194/bg-13-1439-2016.

Hennekens, S.M., and Schaminée, J.H.J. 2001. TURBOVEG, a comprehensive data base management system for vegetation data. J. Veg. Sci. **12**: 589–591. doi:10.2307/3237010.

Jones, B.M., Amundson, C.L., Koch, J.C., and Grosse, G. 2013. Thermokarst and thaw-related landscape dynamics—An annotated bibliography with an emphasis on potential effects on habitat and wildlife: U.S. Geological Survey Open-File Report 2013-1161, 60 p., Available from: http://pubs.usgs.gov/of/2013/1161.

Jones, F.C. 2016. Cumulative effects assessment: theoretical underpinnings and big problems. Environ. Rev. **1**; 24(2): 187–204. doi: 10.1139/er-2015-0073

Jorgenson, J.C., Raynolds, M.K., Reynolds, J.H., and Benson, A.-M. 2015b. Twenty-five year record of changes in plant cover on tundra of northeastern Alaska. Arct. Antarct. Alp. Res. **47**: 785–806. doi:10.1657/AAAR0014-097.

Jorgenson, J.C., Jorgenson, M.T., Boldenow, M.L., and Orndahl, K.M. 2018. Landscape change detected over a half century in the Arctic National Wildlife Refuge using high-resolution aerial imagery. Remote Sens. **10**: 1305. doi:10.3390/rs10081305.

M.T. Jorgenson(ed). 2011. Coastal region of northern alaska: guidebook to permafrost and related features. Guidebook 10 prepared for the Ninth International Conference on Permafrost, June 29 –3 July 2008. Fairbanks, AK: Alaska Division of Geophysical and Geological Surveys. 188pp. Available from: https://www.arlis.org/docs/vol1/E/754862935.pdf.

Jorgenson, M.T., and Joyce, M.R. 1994. Six strategies for rehabilitating land disturbed by oil development in Arctic Alaska. Arctic. **47**: 374–390. doi: 10.14430/arctic1311

Jorgenson, M.T., Shur, Y.L., and Pullman, E.R. 2006. Abrupt increase in permafrost degradation in Arctic Alaska. Geophys. Res. Lett. **25**: L02503. doi: 10.1029/2005GL024960.

Jorgenson, M.T., Kanevskiy, M., Shur, Y., Moskalenko, N., Brown, D.R.N., Wickland, K., Striegl, R., and Koch, J. 2015a. Role of ground ice dynamics and ecological feedbacks in recent ice wedge degradation and stabilization. J. Geophys. Res.-Earth. **120**: 2280–2297. doi:10.1002/2015JF003602.

Kanevskiy, M., Shur, Y., Jorgenson, M.T., Ping, C.-L., Michaelson, G.J., Fortier, D., Stephani, Dillon, and Tumskoy,, M. 2013. Ground ice in the upper permafrost of the Beaufort Sea coast of Alaska. Cold Reg. Sci. Technol. **85**: 56–70. doi: 10.1016/j.coldregions.2012.08.002

Kanevskiy, M., Shur, Y., Jorgenson, M.T., Brown, D.R.N., Moskalenko, N., Brown, J., Walker, D.A., et al. 2017. Degradation and stabilization of ice wedges: implications for assessing risk of thermokarst in northern Alaska. Geomorphol. **297**: 20–42. doi: 10.1016/j.geomorph.2017.09.001.

Kanevskiy, M., Shur, Y., Walker, D.A., Jorgenson, T., Raynolds, M.K., Wirth, L.M., Jones, B., et al. 2022. Cryostratigraphy of the upper permafrost and risk of ice-wedge thermokarst in relation to road infrastructure, Prudhoe Bay Oilfield, Alaska. Arct. Sci. **8** (3):498–530. doi:10.1139/as-2021-0024.

Kidd, J.G., Streever, W., and Jorgenson, M.T. 2006. Site characteristics and plant community development following partial gravel removal in an Arctic oilfield. Arctic, Antarctic, and Alpine Research. **38**: 384–393. doi:10.1657/1523-0430(2006)38[384:SCAPCD]2.0.CO;2.

Koch, J.C., Jorgenson, M.T., Wickland, K.P., Kanevskiy, M., and Striegl, R. 2018. Ice wedge degradation and stabilization impacts water budgets and nutrient cycling in Arctic trough ponds. J. Geophys. Res.- Biogeosci. **123**: 2604–2616. doi:10.1029/2018JG004528.

Kruskal, J.B. 1964. Numeric multidimensional scaling: a numerical method. Psychometrika. **29**: 1–27. doi: 10.1007/BF02289565

Langer, M., Westermann, S., Boike, J., Kirllin, G., Peng, S., and Krinner, G. 2016. Rapid degradation of permafrost underneath waterbodies in tundra landscapes—toward a representation of thermokarst in land surface models. J. Geophys. Res.-Earth. **121**: 2446–2470. doi:10.1002/2016JF003956.

Liljedahl, A.K., Boike, J., Daanen, R.P., Fedorov, A.N., Frost, G.V., Grosse, G., Hinzman, L.D., et al. 2016. Pan-Arctic ice-wedge degradation in warming permafrost and its influence on tundra hydrology. Nat. Geosci. **9**: 312–318. doi:10.1038/ngeo2674.

Maki, A.W. 1992. Of measured risks: the environmental impacts of the Prudhoe Bay, Alaska, oil field. Environ. Toxicol. Chem. **12**: 1691–707. doi:10.1002/etc.5620111204.

McCune, B., Grace, J.B., and Urban, D.L. 2002. Analysis of ecological communities. Gleneden Beach, OR: MJM Software Design. Available from: https://www.wildblueberrymedia.net/analysis-of-ecological-communities.

Melvin, A.M., Larsen, P., Boehlert, B., Neumann, J.E., Chinowsky, P., Espinet, X., et al. 2017. Climate change damages to Alaska public infrastructure and the economics of proactive adaptation. PNAS. **114**(2): E122–31. doi: 10.1073/pnas.1611056113

Myers-Smith, I.H., Arnesen, B.K., Thompson, R.M., and Chapin, F.S. 2006. Cumulative impacts on Alaskan arctic tundra of a quarter century of road dust. Écoscience. **13**(4): 503–510. doi: 10.2980/1195-6860(2006)13[503:CIOAAT]2.0.CO;2.

Myers-Smith, I.H., Forbes, B.C., Wilmking, M., Hallinger, M., Lantz, T., Blok, D., Tape, K.D., et al. 2011. Shrub expansion in tundra ecosystems: dynamics, impacts, and research priorities. Envir. Res. Lett. **6**: 045509. doi: 10.1088/1748-9326/6/4/045509

Myers-Smith, I.H., Elmendorf, S.C., Beck, P.S.A., Wilmking, M., Hallinger, M., Blok, D., Tape, K.D., et al. 2015. Climate sensitivity of shrub growth across the tundra biome. Nat. Clim. Change. **5**(9): 887–891. doi: 10.1038/nclimate2697

NRC (National Research Council). 2003. Cumulative environmental effects of oil and gas activities on Alaska's North Slope. National Academies Press, Washington DC. doi: 10.17226/10639.

Naito, A.T., and Cairns, D.M. 2015. Patterns of shrub expansion in Alaskan arctic river corridors suggest phase transition. Ecol. Evol. **5**(1): 87–101. doi:10.1002/ece3.1341.

Nelson, F.E., Anisimov, O.A., and Shiklomanov, N.I. 2001. Subsidence risk from thawing permafrost – the threat to man-made structures across regions in the far north can be monitored. Nature. **410**: 889–890. doi: 10.1038/35073746

Nitzbon, J., Langer, M., Westermann, S. Martin, L., Aas, K.S., and Boike, J., 2019. Pathways of ice-wedge degradation in polygonal tundra under different hydrological conditions. The Cryosphere. **13**(4): 1089–1123. doi:10.5194/tc-13-1089-2019.

Nitzbon, J., Westermann, S., Langer, M., Martin, L.C.P., Strauss, J., Laboor, S., and Boike, J. 2020. Fast response of cold ice-rich permafrost in northeast Siberia to a warming climate. Nat. Commun. **11**: 2201. doi:10.1038/s41467-020-15725-8.

Perreault, N., Lévesque, E., Fortier, D., and Lamarque, L.J. 2016. Thermoerosion gullies boost the transition from wet to mesic tundra vegetation. Biogeosciences. **13**: 1237–1253. doi: 10.5194/bg-13-1237-2016

Povoroznyuk, O., Vincent, W.F., Schweitzer, P., Laptander, R., Bennett, M., Sergeev, D., Forbes, B.C., Roy-Léveillée, P., and Walker, D.A. 2021 submitted. Arctic roads and railways: environmental and social consequences of transport infrastructure in the circumpolar north. Arct. Sci. doi:10.1139/as-2021-0033.

Rawlinson, S.E. 1993. Surficial geology and morphology of the Alaskan central Arctic coastal plain. Alaska Division of Geology and Geophysical Surveys, Report of Investigations RI 93-1, 172pp. Available from: https://doi.org/10.14509/2484.

Raynolds, M.K., Walker, D.A., Ambrosius, K.J., Brown, J., Everett, K.R., Kanevskiy, M., Kofinas, G.P., Romanovsky, V.E., Shur, Y., and Webber, P.J. 2014a. Cumulative geoecological effects of 62 years of infrastructure and climate change in ice-rich permafrost landscapes, Prudhoe Bay Oilfield, Alaska . Glob. Change Biol. **20**: 1211–1224. doi:10.1111/gcb.12500.

Raynolds, M.K., Walker, D.A., Buchhorn, M., and Wirth, L.M. 2014b. Vegetation changes related to 45 years of heavy road traffic along the spine road at Prudhoe Bay, Alaska. Poster presented at Arctic Change 2014. Ottawa, ON December 8-12. Abstract 333. Available from: https://www.geobotany.uaf.edu/library/posters/Raynolds2014_OttawaAC2014_pos20141205.

Raynolds, M.K., Jorgenson, J.C., Jorgenson, M.T., Kanevskiy, M., Liljedahl, A.K., Nolan, M., Sturm, M., and Walker, D.A. 2020. Landscape impacts of 3D-seismic surveys in the Arctic National Wildlife Refuge, Alaska. Ecol. Appl. **30**: eap.2143. doi: 10.1002/eap.2143.

Richardson, D.H.S. 1974. A report on the lichens at Prudhoe Bay, Alaska, U.S.A. as monitors of air quality. Unpublished report to the U.S. Tundra Biome. Sudbury, Ontario: Laurentian University, 16pp. Provided by the author in personal communication July 1974.

Roback, A. 2002. The climatic aftermath. Science, **295**: 242–244. Available from: https://www.science.org/doi/10.1126/science.1069903.

Romanovsky, V.E., and Osterkamp, T.E. 1995. Interannual variations of the thermal regime of the active layer and near-surface permafrost in Northern Alaska. Permafrost Periglac. **6**: 313–335. doi:10.1002/ppp.3430060404.

Romanovsky, V., Isaksen, K., Drozdov, D., Anisimov, O., Instanes, A., Leibman, M., et al. 2017. Changing permafrost and its impacts. *In* Snow, Water, Ice and Permafrost in the Arctic (SWIPA). Arctic Monitoring and Assessment Programme (AMAP), Oslo, Norway. pp. 65–102. Available from: https://www.amap.no/documents/doc/snow-water-ice-and-permafrost-in-the-arctic-swipa-2017/1610.

Schneider von Deimling, T., Lee, H., Ingeman-Nielsen, T. Westermann, S., Romanovsky, V., Lamoureux, S., Walker, D.A., Chadburn, S., Trochim, E., Cai, L., Nitzbon, J., Jacobi, S., and Langer, M. 2021. Consequences of permafrost degradation for Arctic infrastructure – bridging the model gap between regional and engineering scales. The Cryosphere. **15**: 2451–2471. doi:10.5194/tc-15-2451-2021.

Seaward, M.R.D. 1993. Lichens and sulphur dioxide air pollution: field studies. Environ. Rev. **1**: 73–91. doi:10.1139/a93-007.

Streever, B., Suydam, R., Shuchman, R., Payne, J.F., Shuchman, R., Angliss, R.P., Balogh, G., Brown, J., Grunblatt, J., Guyer, S., Kane, D.L., Kelley, J.J., Kofinas, G., Lassuy, D.R., Loya, W., Martin, P., Moore, S.E., Pegau, W.S., Rea, C., Reed, D.J., Sformo, T., Sturm, M., Taylor, J.J., Viavant, T., Williams, D., and Yokel, D. 2011. Environmental change and potential impacts: applied research priorities for Alaska's North Slope. Arctic. **64**: 390–397. doi:10.14430/arctic4137.

Sturm, M., Racine, C., and Tape, K. 2001. Increasing shrub abundance in the Arctic. Nature. **411**: 546–547. doi: 10.1038/35079180

Tape, K., Sturm, M., and Racine, C. 2006. The evidence for shrub expansion in Northern Alaska and the Pan-arctic. Global Change Biol. **12**: 686–702. doi:10.1111/j.1365-2486.2006.01128.x.

Thoman, R.J. 1995. The climate of Prudhoe Bay, Alaska. Anchorage: National Weather Service Regional Headquarters, NOAA Technical Memorandum NWS AR-44, pp. 1–15. Provided by author in personal communication: email 2 August 2020.

Tichý, L., Holt, J., and Nejezchlebova, M. 2011. JUICE program for management, analysis and classification of ecological data. 1st and 2nd parts. Brno: Vegetation Science Group. Masaryk University. Available from: https://www.sci.muni.cz/botany/juice/JCman2011_1st.pdf, https://www.sci.muni.cz/botany/juice/JCman2011_2nd.pdf.

Tichý, L. 2002. JUICE, software for vegetation classification. J. Veg. Sci. **13**(3): 451–453. doi: 10.1111/j.1654-1103.2002.tb02069.x

J.C. Truett and S.R. Johnson(eds.) 2000. The natural history of an Arctic oil field: Development and the Biota. San Diego: Academic Press. Available from: https://www.elsevier.com/books/the-natural-history-of-an-arctic-oil-field/truett/978-0-12-701235-3.

Truett, J.C., Miller, M.E., and Kertell, K. 1997. Effects of arctic Alaska oil development on brant and snow geese. Arctic. **50**: 138–146. doi:10.14430/arctic1096.

Van der Sluijs, J., Kokelj, S.V., Fraser, R.H., Tunnicliffe, J., and Lacelle, D. 2018. Permafrost terrain dynamics and infrastructure impacts revealed by UAV photogrammetry and thermal imaging. Remote Sens. **10**(11): 1734. doi:10.3390/rs10111734.

Vincent, W.F., Lemay, M., and Allard, M. 2017. Arctic permafrost landscapes in transition: towards an integrated earth system approach. Arct. Sci. **3**: 39–64. doi:10.1139/as-2016-0027.

Vincent, W.F., Canário, J., and Boike, J. 2019. Understanding the terrestrial effects of Arctic sea ice decline. Eos. **100**: 17 July 2019. doi:10.1029/2019EO128471.

Vonk, J.E., Tank, S.E., Bowden, W.B., Laurion, I., Vincent, W.F., Alekseychik, P., Amyot, et al. 2015. Reviews and syntheses: effects of permafrost thaw on Arctic aquatic ecosystems. Biogeosciences. **12**: 7129–7167. doi: 10.5194/bg-12-7129-2015.

Walker, D.A. 1985. Vegetation and environmental gradients of the Prudhoe Bay Region, Alaska. CRREL Report 85-14, Hanover, NH: U.S. Army Cold Regions Research and Engineering Laboratory, 240pp. Available from: https://hdl.handle.net/11681/9420.

Walker, D.A. 2016. Arctic vegetation plots, Prudhoe Bay, AK, 1973–1980, Oak Ridge, Tennessee: ORNL DAAC. doi: 10.3334/ORNLDAAC/1360.

Walker, D.A. 2017. Arctic vegetation plots, Prudhoe Bay ArcSEES Road Study, Lake Colleen, 2014. Oak Ridge, Tennessee: ORNL DAAC. Available from: https://daac.ornl.gov/ABOVE/guides/Prudhoe_Bay_ArcSEES_Veg_Plots.html.

Walker, D.A. 1996. Disturbance and recovery of arctic Alaskan vegetation. In Landscape function and disturbance in Arctic tundra. *Edited by* J.F. Reynolds and J.D. Tenhunen. Springer Verlag, Berlin-Heidelberg. pp. 36–71. Available from: https://www.springer.com/gp/book/9783662011478.

Walker, D.A., and Everett, K.R. 1987. Road dust and its environmental impact on Alaskan taiga and tundra. Arct. Alp. Res. **19**: 479–489. doi: 10.2307/1551414

Walker, D.A., and Everett, K.R. 1991. Loess ecosystems of northern Alaska: regional gradient and toposequence at Prudhoe Bay. Ecol. Monogr. **61**: 437–464. doi:10.2307/2937050.

D.A. Walker and J.L. Peirce(eds.) 2015. Rapid arctic transitions due to infrastructure and climate (RATIC): a contribution to ICARP III. AGC 16-02, Fairbanks, AK: Alaska Geobotany Center, 51pp. Available from: https://www.geobotany.uaf.edu/library/pubs/WalkerDAed2015-RATICWhitePaper-ICARPIII.pdf.

Walker, D.A., and Webber, P.J. 1980. Vegetation. *In* Geobotanical atlas of the Prudhoe Bay region, Alaska. *Edited by* D.A. Walker, K.R. Everett, P.J. Webber and J. Brown. U.S. Army Corps of Engineers, Cold Regions Research and Engineering Laboratory, Hanover, NH. pp. 24–34. CRREL Report 80-14. Available from: https://hdl.handle.net/11681/9008.

D.A. Walker, K.R. Everett, P.J. Webber and J. Brown(eds.) 1980. Geobotanical Atlas of the Prudhoe Bay region, Alaska. CRREL Report 80-14. Cold Regions Research and Engineering Laboratory, Hanover, NH. Available from: https://hdl.handle.net/11681/9008.

Walker, D.A., Webber, P.J., Walker, M.D., Lederer, N.D., Meehan, R.H., and Nordstrand, E.A. 1986. Use of geobotanical maps and automated mapping techniques to examine cumulative impacts in the Prudhoe Bay Oilfield, Alaska. Environ. Conserv. **13**: 149–160. doi: 10.1017/S0376892900036754

Walker, D.A. Cate, D., Brown, J., and Racine, C. 1987a. Disturbance and recovery of arctic Alaskan tundra terrain: a review of recent investigations. Hanover, NH: U.S. Army Cold Regions Research and Engineering Laboratory, CRREL Report 87-11, 63pp. Available from https://hdl.handle.net/11681/9030.

Walker, D.A., Webber, P.J., Binnian, E.F., Everett, K.R., Lederer, N.D., Nordstrand, E.A., and Walker, M.D. 1987b. Cumulative impacts of oil fields on northern Alaskan landscapes. Science. **238**: 757–761. doi: 10.1126/science.238.4828.757.

Walker, D.A., Buchhorn, M., Kanevskiy, M., Matyshak, G.V., Raynolds, M.K., Shur, Y.L., and Wirth, L.M. 2015. Infrastructure-thermokarst-soil-vegetation interactions at Lake Colleen Site A, Prudhoe Bay, Alaska. Alaska Geobotany Center, AGC 15-01, Fairbanks, AK. 92pp. doi: 10.18739/A2M61BQ8M.

Walker, D.A., Kanevskiy, M.K., Shur, Y.L., Raynolds, M.K., Peirce, J.L., Buchhorn, M., Ermokhina, K., and Druckenmiller, L.A. 2018. 2016

ArcSEES data report: snow, thaw, temperature, and permafrost borehole data from the Colleen & Airport sites, Prudhoe Bay, and photos of the Quintillion fiber optic cable impacts, North Slope, Alaska. Alaska Geobotany Center, AGC 18-01, Fairbanks, AK. 66pp. Available from: https://arcticdata.io/catalog/view/doi%3A10.18739%2FA28K74×6T.

Watson-Cook, E., Walker, D.A., Raynolds, M.K., and Breen, A.L. 2021. Thermokarst pond plant communities of Prudhoe Bay, Alaska: environmental gradients and temperature feedbacks. Boulder, CO, 50th International Arctic Workshop. Available from https://instaar.colorado.edu/meetings/AW2021/abstract_details.php?abstract_id=38.

Webber, P.J., and Walker, D.A. 1975. Vegetation and landscape analysis at Prudhoe Bay, Alaska: a vegetation map of the Tundra Biome study area. *In* Ecological investigations of the Tundra Biome in the Prudhoe Bay Region. *Edited by* J Brown.Biological Papers of the University of Alaska, pp. 80–91. Special Report 2. Available from: https://www.arlis.org/docs/vol1/B/3035866.pdf.

Westhoff, V., and Van der Maarel, E., 1978. The Braun-blanquet approach. *In* Classification of Plant Communities. *Edited by* R.H. Whittaker, W. Junk, and Den Haag, pp. 287–399. Available from: https://www.springer.com/gp/book/9789061935667.

Wickland, K.P., Jorgenson, M.T., Koch, J.C., Kanevskiy, M., and Striegl, R.G. 2020. Carbon dioxide and methane flux in a dynamic arctic tundra landscape: decadal-scale impacts of ice wedge degradation and stabilization. Geophys. Res. Lett. **47**: 75. doi:10.1029/2020GL089894.

Witharana, C., Bhuiyan, M.A.E., Liljedahl, A.K., Kanevskiy, M., Jorgenson, M.T., Jones, B.M., et al. 2021. An object-based approach for mapping tundra ice-wedge polygon troughs from very high spatial resolution optical satellite imagery. Remote Sens. **13**: 558. doi:10.3390/rs13040558.